Check for updates

Photodegradation of some brominated and phenolic micropollutants in raw hospital wastewater with CeO_2 and TiO_2 nanoparticles

Delia Teresa Sponza and Gökçe Güney

ABSTRACT

In this study, the degradations of 2,3,4,5,6-pentabromotoluene (PBT), 2,3,4,5,6-pentabromoethyl benzene (PBEB), triclosan (TCS) and gemfibrozil (GFZ) in raw hospital wastewater were investigated with cerium (IV) oxide and titanium (IV) oxide nanoparticles considering the mechanisms of adsorption, photolysis, and photocatalysis with UV-C lamps. The effects of nano-CeO_2 and nano-TiO_2 concentrations, irradiation times, UV light powers and hospital wastewater pH on the photodegradation yields of micropollutants namely PBT, PBEB, TCS and GFZ were investigated throughout photocatalysis. The nano-TiO_2 produced had an anatase phase with crystalline shape with a surface area of 205 $m^2\ g^{-1}$ and an average size of 11.50 nm. The CeO_2 nanoparticles had a spherical shape with a higher surface area (302 $m^2\ g^{-1}$) than that of TiO_2 and a lower average size (8.11 nm). It was found that the removals of PBT, PBEB, TCS and GFZ with adsorption (5.7%–17.1%) and photolysis (9.0%–15.9%) were not significant for both nanoparticles. The photodegradation of PBT (92%), PBEB (90%), TCS (97%) and GFZ (95%) with nano-CeO_2 gave better results than nano-TiO_2 (90%, 87%, 94% and 93% for PBT, PBEB, TCS and GFZ, respectively) under optimum experimental conditions (0.50 g L^{-1} nano-CeO_2, 45 min irradiation time, 25 °C temperature, pH = 8.50, 210 W UV light power). Both nanoparticles were reused effectively after photo-removals of the micropollutants from the hospital wastewater. The lowest photodegradation yields were 80%, 78%, 75% and 74% for TCS, GFZ, PBT and PBEB, respectively, with nano-TiO_2 after six sequential treatments. The lowest photodegradation yields were 86%, 83%, 80% and 79% for the same micropollutants, respectively, with nano-CeO_2 after six sequential treatments. The cost to treat 1 m^3 raw hospital wastewater were 8.70 € and 2.28 €, for the photocatalytic treatments with nano-TiO_2 and nano-CeO_2, respectively.

Key words | hospital wastewater, micropollutants, nanoparticles, photocatalytic

Delia Teresa Sponza (corresponding author)
Gökçe Güney
Environmental Engineering Department,
Engineering Faculty,
Dokuz Eylul University,
Tinaztepe Campus,
Buca,
Izmir 35160,
Turkey
E-mail: *delya.sponza@deu.edu.tr*

INTRODUCTION

Micropollutants in hospital wastewater are directly discharged into the sewage system without treatment since the conventional sewage/urban treatment plants can only remove macropollutants such as biochemical oxygen demand, chemical oxygen demand (COD), nitrogen and phosphorus in Turkey. The micropollutants decrease the biological treatment efficiency if they are not treated and then discharged into the receiving environment (Petrie *et al.* 2014).

Gemfibrozil (GFZ) is a blood lipid regulator and is used to treat hypertriglyceridemia (Grenni *et al.* 2013). It is frequently detected in surface water and wastewater (Krkošek *et al.* 2011). GFZ is toxic to aquatic microorganisms and may also cause endocrine disruption in fish (Chen *et al.* 2017). It has been found in wastewater treatment plants and also in freshwaters at a concentration ranging from 0.07 to 0.51 μg L^{-1} (Fang *et al.* 2012). Triclosan (TCS) is a broad-spectrum antibacterial and antifungal agent (Xie *et al.* 2012) used in hospitals. It has been found in surface waters, wastewaters, sediments and sludges due its widespread usage. It has low acute and chronic toxicities (Tohidi & Cai 2017). The concentration of TCS has been found to range from 1.4 up to 133,000 ng L^{-1} in surface waters, and from 20 to 133,000 μg kg^{-1} dw in biosolids (Montaseri & Forbes 2016). 2,3,4,5,6-Pentabromoethyl benzene (PBEB) and 2,3,4,5,6-pentabromotoluene (PBT) are new brominated

doi: 10.2166/wst.2017.433

Downloaded from http://iwaponline.com/wst/article-pdf/76/10/2603/242040/wst076102603.pdf
by guest

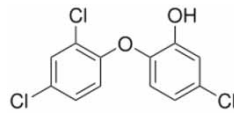
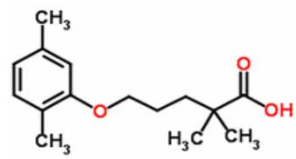
flame retardants (NBFRs) and have been used in order to prevent fires and in the formation of different types of polymers, resins and plastics (Cristale *et al.* 2012; Chen *et al.* 2012). NBFRs are of environmental concern because of their high lipophilicity, persistence and resistance to degradation (Barón *et al.* 2015). Their bioaccumulative and carcinogenic/mutagenic properties make them potentially dangerous for environmental health (Sun *et al.* 2015). PBEB was detected in samples of river sediments at concentrations ranging from 3.1 to 10.0 ng g^{-1} dry weight (Cristale *et al.* 2013). In river water, PBT concentrations range from 0.0003 to 0.0210 μg L^{-1} (Wu *et al.* 2010).

Nanoparticles with unique surface-active properties are beneficial in removing pharmaceuticals and micropollutants (Hu *et al.* 2012). Titanium (IV) oxide (TiO_2) as a photocatalyst is widely applied to wastewater treatment due to its photocatalytic oxidation ability, and stable and non-toxic characteristics (Chen *et al.* 2017). Cerium (IV) oxide (CeO_2) nanoparticles are widely used as a catalyst and as superconducting materials (Xu *et al.* 2017).

The treatability studies of GFZ, TCS, PBT and PBEB performed with nano-CeO_2 and nano-TiO_2 via photocatalytic processes are limited in recent literature. Chen *et al.* determined 61.8% GFZ removal with 0.05 g L^{-1} nano-TiO_2 in a synthetic wastewater having a GFZ concentration of 2 mg L^{-1} under 350 W UV light power at a pH of 7.00 through 8.0 min (Chen *et al.* 2017). Son *et al.* reported 82% TCS photodegradation rate within 20 min with 0.1 g L^{-1} nano-TiO_2 at a pH of 7.00 under 1.37×10^{-4} Einstein L^{-1} min^{-1} UV (Son *et al.* 2009). Yu *et al.* found 95% photocatalytic degradation for 9 mg L^{-1} TCS within 6 h using 100 mg L^{-1} nano-TiO_2 at UV light power of 15 W (Yu *et al.* 2006). García *et al.* found 85% TCS photodegradation at 100 μg L^{-1} TCS by 0.335 g L^{-1} nano-TiO_2 under solar light irradiation after 120 min (García *et al.* 2012). The physicochemical properties (hydrophobicity, solubility, volatilization) of micropollutants used in this study are shown in Table 1.

The novelty of the study is to treat some brominated and phenolic micropollutants present in raw hospital wastewater for the first time in Turkey by photocatalytic processes under laboratory conditions. The aim of this study was to evaluate the photocatalytic removals of PBT, PBEB, TCS and GFZ in a raw hospital wastewater using CeO_2 and TiO_2. Effects of irradiation times (15; 30; 45; 60; 90 min), nanoparticle concentrations (0.25; 0.50; 1.00; 1.50 g L^{-1}), UV light powers (120; 210; 300 W) and raw hospital wastewater pH (4.00; 7.00; 8.50) on PBT, PBEB, TCS and GFZ photodegradation yields throughout photocatalysis at constant temperature (25 °C) were investigated using nano-CeO_2 and nano-TiO_2

Table 1 | Physicochemical properties of PBEB, PBT, TCS and GFZ (from US Environmental Protection Agency EPI Suite™ database, 2017)

IUPAC name	Abbreviation	Molecular weight (g mol^{-1})	Henry's Law constant, k_H at 25 °C (atm m^3 mol^{-1})	Solubility in water, at 25 °C (g L^{-1})	Dissociation constant, pK_a (unitless)	Octanol/water partition coefficient, log K_{ow}	Structure
2,3,4,5,6-pentabromoethyl benzene (CAS No. 85-22-3)	PBEB	500.65	1.12×10^{-4}	2.895×10^{-7}	N.A.	7.48	
2,3,4,5,6-pentabromotoluene (CAS No. 87-83-2)	PBT	486.62	7.22×10^{-5}	9.351×10^{-7}	N.A.	6.99	
5-chloro-2-(2,4-dichloro-phenoxy)-phenol (CAS No. 3380-34-)	TCS	289.55	2.13×10^{-8}	4.621×10^{-3}	7.9	4.76	
5-(2,5-dimethyl phenoxy)-2,2-dimethyl pentanoic acid (CAS No. 25812-30-0)	GFZ	250.34	1.19×10^{-8}	4.964×10^{-3}	4.5	4.77	

N.A. Not available.

Downloaded from http://iwaponline.com/wst/article-pdf/76/10/2603/242040/wst076102603.pdf
by guest

generated under laboratory conditions. The recoveries of the nanoparticles and their costs were also investigated.

MATERIALS AND METHODS

Source and characterization of raw hospital wastewater

Raw hospital wastewater was taken from the Dokuz Eylul University Hospital (Izmir, Turkey) sewer channel, which flows through the sewer channel without any treatment. The influent COD concentration of the raw hospital wastewater was $1{,}900 \pm 20$ mg L^{-1} while the influent PBT, PBEB, TCS and GFZ concentrations were 2.31 ± 0.003, 3.28 ± 0.004, 860.00 ± 0.05 and 53.30 ± 0.05 μg L^{-1}, respectively. The pH, the temperature, the total nitrogen and total phosphorus concentrations were 8.50 ± 0.02, 18 ± 2 °C, 0.40 ± 0.01 and 1.00 ± 0.01 mg L^{-1}, respectively.

Analytical procedure

Extraction of PBEB, PBT, TCS and GFZ from raw hospital wastewater

PBEB, PBT, TCS and GFZ were extracted the from raw hospital wastewater by solid-phase extraction method. Oasis HLB cartridges (200 mg) were used in the extraction experiments. PBEB and PBT extraction experiments were carried out according to Chokwe *et al.* (2015) while TCS and GFZ extraction experiments were carried out according to Diwan *et al.* (2010). Extraction recovery rates for PBEB, PBT, TCS and GFZ are shown in Table 2.

PBEB, PBT, TCS and GFZ measurement in raw hospital wastewater

PBEB (CAS No. 85-22-3) and PBT (CAS No. 87-83-2) measurements were performed on a GC Agilent 7890A equipped with an Agilent 5975C inert mass selective detector. The gas chromatography–mass spectrometer (GC-MS) is equipped with a flame ionization detector and an HP-5MS capillary column with dimensions of 30.0 m (length), 0.250 mm (I.D.), and 0.25 μm (film thickness) from Agilent Technologies. The oven program was taken from Cristale *et al.* and developed as following: the oven was set at 40 °C (1 min), increased to 60 °C at 15 °C min^{-1} (8 min), to 220 °C at 10 °C min^{-1} and to 300 °C at 15 °C min^{-1} (8 min). Helium (purity 99.999%) was employed as carrier

Table 2 | The RT, m/z transitions, extraction and method recovery rates for PBEB, PBT, TCS and GFZ

Compound	Retention time (min)	m/z transitions			Recovery study							
		Ion 1	Ion 2	Ion 3	Actual concentration (μg L^{-1})	Peak area of the standard	Peak area of the sample	Extraction recovery (%)	Determined concentration (μg L^{-1})	Method recovery (%)	Average extraction recovery (%)	Average method recovery (%)
PBEB	10.786	499.7	484.7	486.7	10	49,712	38,777	78.0	6.84	68.4	103.5	91.9
					50	264,915	259,219	97.9	45.71	91.4		
					100	487,294	656,539	134.7	115.76	115.8		
PBT	10.550	485.7	487.7	406.7	10	84,792	64,637	76.2	7.03	70.3	103.3	94.8
					50	437,344	440,972	100.8	47.96	95.9		
					100	818,197	1,087,394	132.9	118.27	118.3		
TCS	3.606	–	–	–	100	2916.30	4163.43	142.8	121.73	121.7	119.07	116.73
					500	14935.00	16405.40	109.8	576.92	115.4		
					1000	29935.00	31301.40	104.6	1130.80	113.1		
GFZ	4.351	–	–	–	100	76.63	73.56	96.00	96.00	96.00	97.35	97.17
					500	563.53	110.45	98.00	490.00	98.00		
					1,000	1008.81	98.92	98.06	975.00	97.50		

Downloaded from http://iwaponline.com/wst/article-pdf/76/10/2603/242040/wst076102603.pdf
by guest

gas with a constant flow of 1.5 mL min^{-1}. The standards were injected (2 μL) into the GC system in splitless mode, with a splitless time of 1.5 min. The injector, quadrupole and transfer line were set at 300, 150, and 280 °C respectively (Cristale *et al.* 2012). The retention times (RT), m/z transitions and method recovery rates for PBEB and PBT monitored by the GC-MS are shown in Table 2.

TCS (CAS No. 3380-34-5) and GFZ (CAS No. 25812-30-0) measurements were performed on an Agilent 1100 Series high-performance liquid chromatograph (HPLC) equipped with a diode array detector. A Thermo C18 column (5 μm, 250 mm × 4.6 mm, Thermo Scientific) was used and the injection volume of each sample was 20 μL. For TCS, the mobile phase consisted of pure acetonitrile and HPLC grade water (90:10 v:v) with a flow rate of 1.0 mL min^{-1} for a column oven temperature of 40 °C and retention time of 3.606 min (Maaroof & Uysal 2014), while for GFZ, the mobile phase consisted of pure acetonitrile, pure methanol and 0.05 M (pH = 7.00) $NH_4H_2PO_4$ (60:30:10 v:v:v) with a flowrate of 0.8 mL min^{-1} for a column oven temperature of 20 °C and retention time of 4.351 min (Elsherif *et al.* 2013). The RT and method recovery rates of TCS and GFZ monitored by the HPLC are shown in Table 2.

Conventional-pollutants measurement methods

Conventional pollutants in hospital wastewater such as COD were measured according to *Standard Methods* (APHA/AWWA/WEF 2012). Total nitrogen and total phosphorus were measured with reagent kits in a Photometer Nova 60/Spectroquant. The pH and temperature were measured with WTW probes.

Preparation of nanoparticles and characterization

$TiCl_4$ (0.92 mL) was dissolved in 35 mL de-ionized water under an ice water bath, and then 0.8 g of P123 as a structure-directing agent was added into the solution under magnet stirring (Tang *et al.* 2016). When the temperature was raised to 50 °C, the mixture solution was aged for another 12 h. Finally, the solution obtained was dried via lyophilization. The obtained solids were calcined at 300 °C for 2 h, and the final product was named as $P_{0.5}$-TiO_2. One millilitre of po1yoxyethylene octylphenol ether was mixed with 1 mL 1-hexanol and 2.5 mL cyclohexane at a mass ratio of 1:1:2.5, then 0.5 mol L^{-1} $Ce(NO_3)_3{\cdot}6H_2O$ was added to obtain an emulsion (Wang *et al.* 2015). This mixture was aged at the reaction temperature of 300 °C for 3 h before being centrifuged to separate the solid, which was subsequently rinsed and dried to obtain the nano-CeO_2.

Field emission scanning electron microscopy (SEM) with 20.0 kV was used to study the morphology of the synthesized TiO_2 and CeO_2 nanoparticles prepared at 300 °C calcination temperatures. Transmission electron microscopy (TEM) with a Zeiss 80.0 kV was used to analyze the estimated particle size of the TiO_2 and CeO_2. XRD analysis was used to identify the phase composition of the prepared TiO_2 and CeO_2 by means of an X-ray diffractometer with the D/max-2200 PC using a Cu Ka radiation source ($\lambda = 1.541$ Å) at 40.0 kV and 200 mA. The optical properties of absorption were measured by an ultraviolet–visible spectrophotometer (UV-Vis) and Fourier transform infrared (FT-IR) spectroscopy, Perkin Elmer Spectrum BX, using the KBr method. The average crystallite size of the samples was calculated by Scherrer's equation (Equation (1)) using TEM as illustrated below:

$$\Phi = (K \times \lambda) / (\beta \times \cos\theta) \quad (1)$$

where Φ is the crystal size, λ is the wavelength of the X-ray irradiation (0.154 nm), K is taken as 0.89, β is the peak width at half-maximum height and θ is the diffraction angle of the peak of the anatase phase. BET (Brunauer–Emmett–Teller) surface area analysis was used to establish the surface area, total pore volume and average pore diameter of the materials. The band gap energy was calculated according to Equation (2):

$$E_g = 1239.8/\lambda \quad (2)$$

where E_g is the band gap (eV) and λ (nm) is the wavelength of the absorption edge in the spectrum.

Photocatalytic studies

The photocatalytic experiments were carried out in a covered stainless steel system consisting of quartz glass reactors with a volume of 1,000 mL and UV light lamps with a 254 nm wavelength (895.0 mm × 26.0 mm, 30.0 W, 0.36 A, G13 Model, Osram). The light power required was provided by increasing or decreasing the UV lamp numbers. The distance between the UV lamps and quartz glass reactors was 10 cm (Figure 1).

The control experiments were carried out under dark conditions for the study of the adsorption capacity of TiO_2 and CeO_2 nanoparticles. Raw hospital wastewater was first filtered through a 0.45 μm pore sized membrane to remove physical impurities. The nanoparticle was added to the filtered hospital wastewater in a quartz glass reactor and it was stirred at 25 °C. The control for photolysis was carried out under UV light

Downloaded from http://iwaponline.com/wst/article-pdf/76/10/2603/242040/wst076102603.pdf
by guest

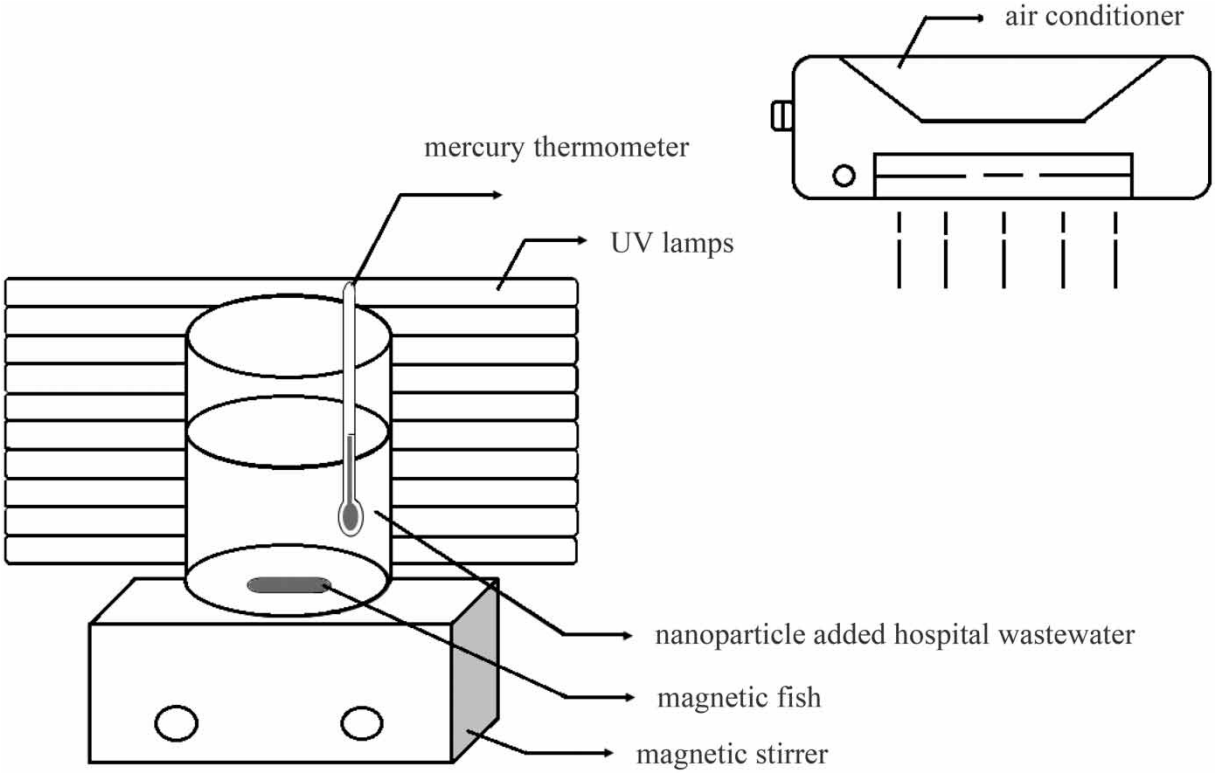


Figure 1 | The photocatalytic reactor system.

without nano-TiO_2 and nano-CeO_2 to determine the photolysis capacity of the micropollutants. Raw hospital wastewater was filtered through a 0.45 μm pore sized membrane and then irradiated under UV in photocatalytic reactors without nanoparticles at 25 °C. All the experiments were performed in triplicate.

The effects of different nanoparticle concentrations (nano-TiO_2 and nano-CeO_2) (0.25; 0.50; 1.00; 1.50 g L^{-1}), irradiation times (15; 30; 45; 60; 90 min), UV light powers (120; 210; 300 W) and hospital wastewater pH (4.00; 7.00; 8.50) on the PBT, PBEB, TCS and GFZ photodegradation yields throughout photocatalysis at constant temperature (25 °C) were investigated.

Recovery and reuse of nanoparticles

After the first utilization of nano-TiO_2 and nano-CeO_2 in the photocatalytic experiments, the nanoparticles were separated by filtering them through 0.45 μm pore sized membranes. Then, the nanoparticles were regenerated using ethanol with 0.10 mol L^{-1} HCl (Chowdhury & Balasubramanian 2014). The nanoparticles were dried under vacuum and they were reused for the second treatment process to treat TCS, GFZ, PBT and PBEB again. For each new treatment step the same procedure was applied to the nanoparticles. Six sequential treatment steps were investigated in order to detect the effect of reusability of the nanoparticles from the raw hospital wastewater after each treatment.

Statistical analysis

The correlation (R) between data was performed using Excel Microsoft 2010 while the significance between parameters was performed in analysis of variance (ANOVA) tests using an α-value of 0.05 with P (probability) values. All of the differences were considered significant at $p < 0.05$. The Kruskal–Wallis one way test was applied to calculate the significant difference of the operational conditions on the photodegradation yields. Kruskal–Wallis ANOVA χ^2 values were calculated for $P > 0.05$(Quinn & Keough 2002).

RESULTS AND DISCUSSION

Physicochemical properties of generated nano metal oxides under laboratory conditions

The SEM image in Figure 2(a) shows that the TiO_2 nanoparticle samples exhibit a well-defined spherical structure after

Downloaded from http://iwaponline.com/wst/article-pdf/76/10/2603/242040/wst076102603.pdf
by guest

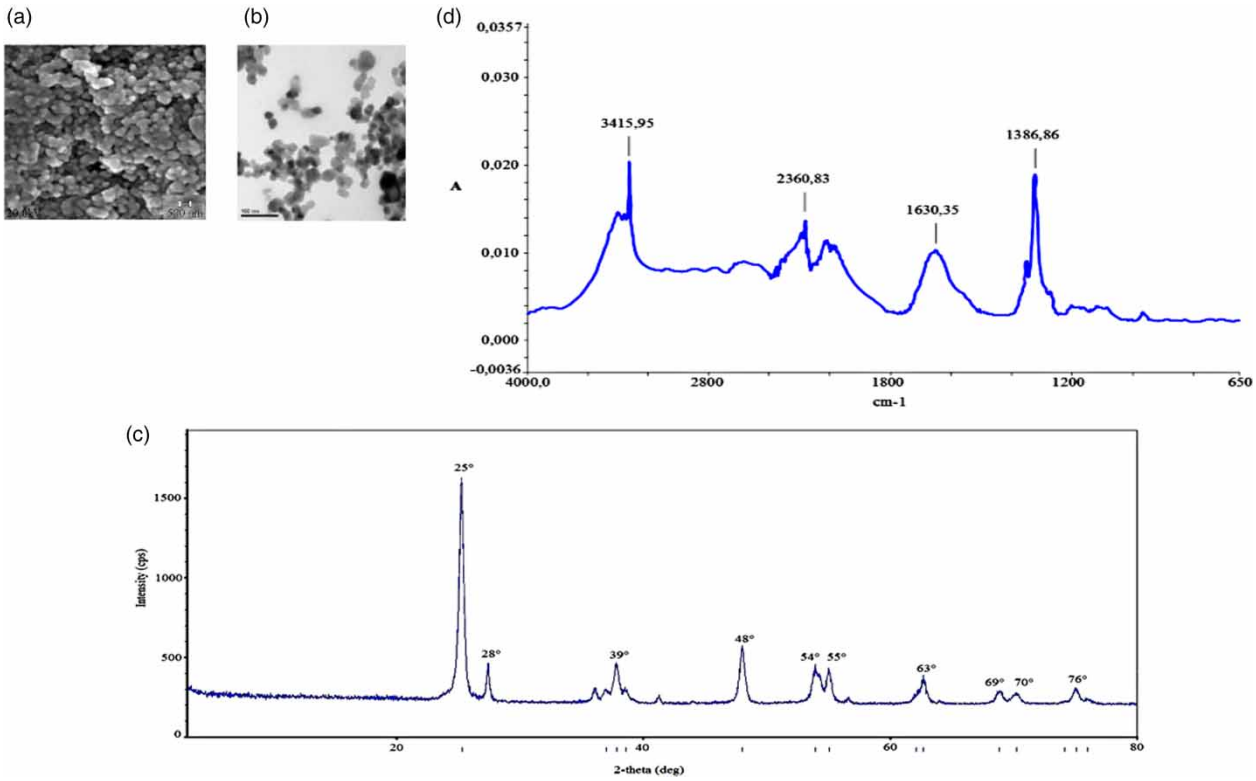


Figure 2 | (a) SEM image, (b) TEM image, (c) XRD analysis and (d) FT-IR peaks of nano-TiO_2 after 45 min irradiation time, at 0.50 g L^{-1} nano-TiO_2 concentration, at 210 W UV light power.

300 °C calcination. The TEM figure shows that the as-prepared powder is completely crystalline, and consists entirely of a pure anatase phase (Figure 2(b)). The XRD analysis showed that the TiO_2 nanoparticle originated completely from the pure anatase phase with a good crystallinity (Figure 2(c)). From the XRD pattern, it is clear that the material formed has a tetragonal crystal structure with lattice parameters a = b = 3.785 Å and c = 9.513 Å. The crystallite size of the TiO_2 was in the range 10.5–11.5 nm and it had a unit cell volume of 136.27 Å (Table 3). The main peaks of anatase TiO_2 appeared at 25°, 28°, 39°, 48°, 54°, 55°, 63°, 69°, 70° and 76° (Figure 2(c)). These peaks of anatase in TiO_2 were in accordance with the peaks given by Hu *et al.* (2017) and Hassani *et al.* (2017) (at 25°, 28°, 38° and 48°, 54°, 55°, 63°, 69°, 70°, and 76°). The strongest and narrowest peaks were detected at $2\theta = 25°$ for anatase. According to FT-IR analysis, the peaks of anatase TiO_2 appeared at 3415.95, 2360.83, 1630.35 and 1386.86 cm^{-1} (Figure 2(d)). These peaks were similar to the findings of Hassani *et al.* (2017). In the FT-IR spectrum of the TiO_2 nanoparticle, the bands appeared at 3415.95–2360.83 cm^{-1}, which shows the bending vibration of OH molecules. A carbonyl peak appeared at around 1630.35 cm^{-1}. The peak at 1386.86 cm^{-1} shows stretching vibrations of Ti-OH. The BET surface area of the synthesized TiO_2 nanoparticle sample shows less aggregation and a smaller particle size, which is in accordance with the SEM and TEM analysis. The BET surface area of the TiO_2 nanoparticle catalyst had an average pore diameter of 98.84 Å with a total pore volume of 0.402 $cm^3\,g^{-1}$ while the surface area was 205 $m^2\,g^{-1}$ (Table 3). The absorption spectrum of the TiO_2 nanoparticle at a wavelength of 410 nm showed that it is a highly crystalline nanomaterial with a band gap value of 3.02 Ev due to the presence of a very fine anatase phase (Figure 2(e)).

Table 3 | BET analysis results and band gap energies of nano-TiO_2 and nano-CeO_2

IUPAC name	Surface area ($m^2\,g^{-1}$)	Pore volume ($cm^3\,g^{-1}$)	Average size (nm)	Pore diameter (Å)
TiO_2	205	0.402	11.50	98.84
Commercial TiO_2	167	0.709	27.00	123.19
CeO_2	302	0.309	8.11	78.06
Commercial CeO_2	319	0.321	9.67	82.90
Sample	**Band gap E_g (eV)**			
TiO_2	3.02			
CeO_2	4.10			

Downloaded from http://iwaponline.com/wst/article-pdf/76/10/2603/242040/wst076102603.pdf
by guest

SEM images showed that CeO_2 nanoparticles exhibited spherical morphologies (Figure 3(a)). Figure 3(b) shows the TEM image of the sample synthesized at 165 °C displaying a particle size of 1–3 nm and strong agglomeration. The XRD patterns reveal that the prepared CeO_2 nanoparticles had a cubic fluorite structure (Figure 3(c)). From the XRD peaks it is evident that the crystallites were oriented along 28°, 33°, 48°, 56°, 59° and 69°, corresponding to the cubic fluorite structure of CeO_2. Similar peaks at 28°, 33°, 48° and 56° were reported by Phuruangrat *et al.* (2017) and Channei *et al.* (2017). The crystallite sizes calculated were around 4.5 and 6.5 nm (Table 2). The BET surface area of the CeO_2 nanoparticle had an average pore diameter of 78.06 Å with a pore volume of 0.309 $cm^3\ g^{-1}$ while the surface area was 302 $m^2\ g^{-1}$ (Table 2). The FT-IR spectrum was recorded in the range of 650 to 4,000 cm^{-1} (Figure 3(d)). These FT-IR peaks are in accordance with the data obtained by Ravishankar *et al.* (2015) and Tambat *et al.* (2016) for CeO_2 nanoparticles). These peaks are due to (Ce-O) metal–oxygen bond vibrations. The band gap of nano-CeO_2 was higher than that of nano-TiO_2 (Table 3). The prepared nano-CeO_2 and nano-TiO_2 exhibited better properties than the commercial nanoparticles (Table 3). Nano-CeO_2 produced under laboratory conditions had a higher surface area than those of nano-TiO_2 while the pore volume, the average size and pore diameter of nano-CeO_2 was lower than nano-TiO_2. This increased the photocatalytic properties of nano-CeO_2. The UV–visible absorption spectral studies showed that the synthesized CeO_2 nanoparticles had a strong absorption band at low wavelength near 380 nm, corresponded to a band gap energy of 3.26 eV (Figure 3(e)). In comparison with the UV–visible absorption spectrum of CeO_2 nanoparticles reported in the literature (Farahmandjou *et al.* 2016), similar peaks in the spectrum located at around 400–700 nm were observed. The high band gap energy and low pore volume and pore diameter of nano-CeO_2 compared to nano-TiO_2 enhanced the UV light absorption of the CeO_2 nanoparticle.

Photocatalytic removal studies

Effect of adsorption alone and photolysis on the removals of GFZ, TCS, PBT and PBEB

During the adsorption studies of micropollutants on the surface of nano-TiO_2 the maximum removal percentages of GFZ, TCS, PBT and PBEB via adsorption were 5.7%, 5.6%, 7.0% and 7.6%, respectively, at 0.50 g L^{-1} nano-TiO_2 concentration after a 45 min stirring time at a pH of 8.50 and a temperature of 25 °C without UV (Figure 4(a)). The adsorption removal percentages of GFZ, TCS, PBT and PBEB were 9.0%, 6.0%, 13.4% and 17.1%, respectively, at 0.50 g L^{-1} nano-CeO_2 concentration after a 45 min stirring time at the same operational conditions given above under dark experimental conditions (Figure 4(b)). It can be said that the adsorption of micropollutants on photocatalyst was not the primary mechanism for their removals. The adsorption yields were double for PBEB and PBT compared to GFZ and TCS. This can be explained by the physicochemical

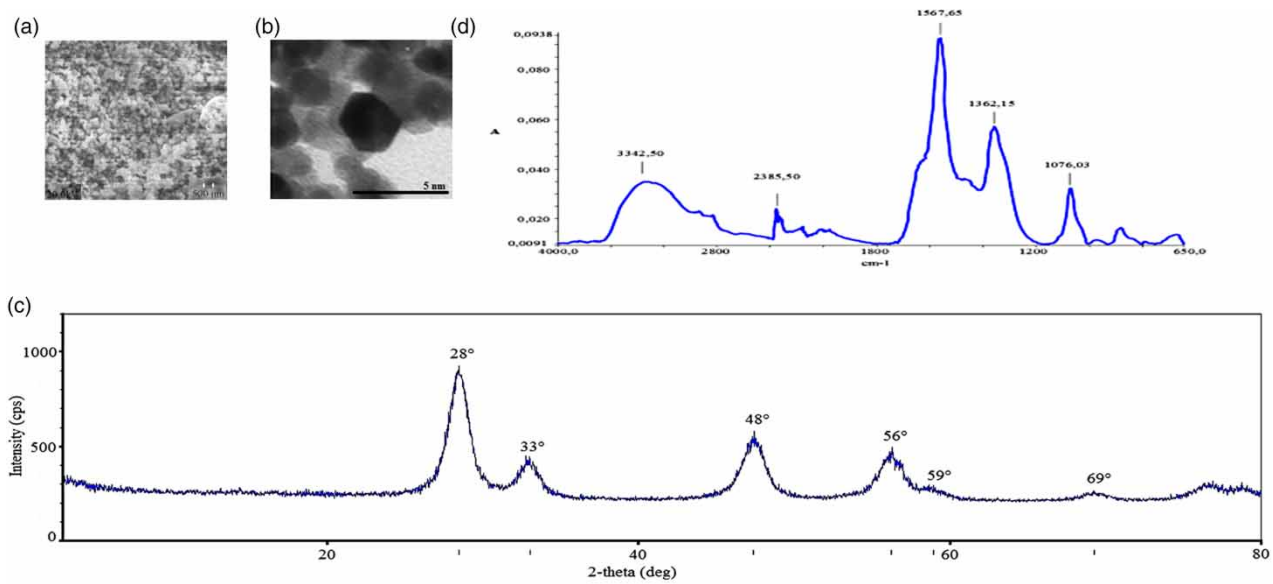
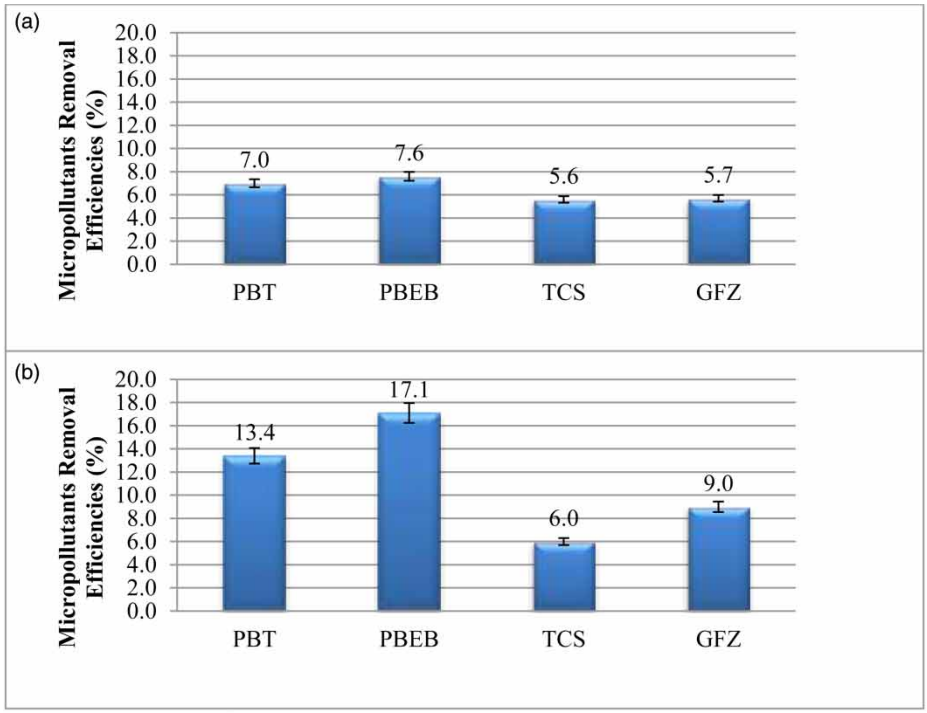
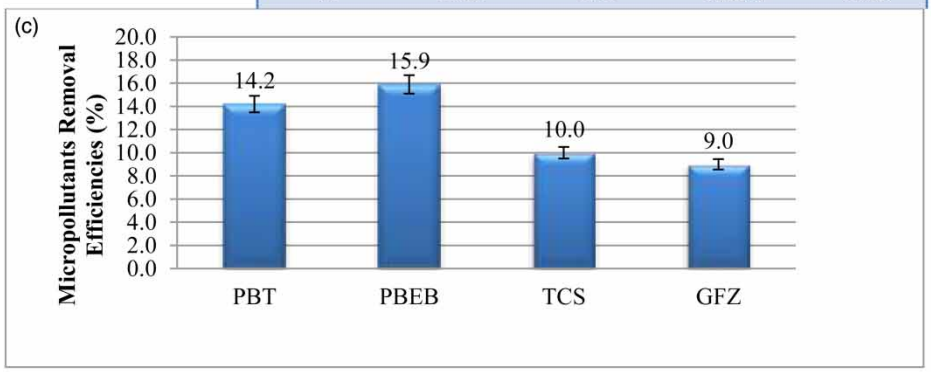


Figure 3 | (a) SEM image, (b) TEM image, (c) XRD analysis and (d) FT-IR peaks of nano-CeO_2 after 45 min irradiation time, at 0.50 g L^{-1} nano-CeO_2 concentration, at 210 W UV light power.

Downloaded from http://iwaponline.com/wst/article-pdf/76/10/2603/242040/wst076102603.pdf
by guest



Concentrations (μg L^{-1})	t (min)	PBT	PBEB	TCS	GFZ
Influent	45	2.31	3.28	860.00	53.30
Effluent for nano-TiO_2	45	2.15	3.03	811.84	50.26
Effluent for nano-CeO_2	45	2.00	2.72	808.40	48.50



Concentrations (μg L^{-1})	t (min)	PBT	PBEB	TCS	GFZ
Influent	45	2.31	3.28	860.00	53.30
Effluent	45	1.98	2.76	774.00	48.50

Figure 4 | (a) The adsorption percentages of GFZ, TCS, PBT and PBEB at 0.50 g L^{-1} nano-TiO_2. (b) The adsorption percentages of GFZ, TCS, PBT and PBEB at 0.50 g L^{-1} nano-CeO_2. (c) The photolysis of GFZ, TCS, PBT and PBEB in the absence of nano-materials.

properties of PBEB (low solubility $= 2.895 \times 10^{-7}$ g L^{-1} and high adsorption capacity log $K_{ow} = 7.48$) and PBT (low solubility $= 9.351 \times 10^{-7}$ g L^{-1} and high adsorption capacity log $K_{ow} = 6.99$) compared to GFZ (low solubility $= 4.964 \times 10^{-3}$ g L^{-1} and high adsorption capacity log $K_{ow} = 4.77$) and TCS (low solubility $= 2.13 \times 10^{-8}$ g L^{-1} and high adsorption capacity log $K_{ow} = 4.76$) and by their structures (brominated groups in PBT and PBEB; phenolic groups in GFZ and TCS). ANOVA multiple regression analysis showed that there was a linear regression between adsorption yields and physicochemical properties of the studied compounds ($R = 0.85$) and this was not statistically significant

Downloaded from http://iwaponline.com/wst/article-pdf/76/10/2603/242040/wst076102603.pdf
by guest

($P = 0.21$, $\alpha = 0.05$). The Kruskal–Wallis one way test showed that the physicochemical properties had a significant effect on adsorption of all micropollutants (Kruskal–Wallis ANOVA, $\chi^2 = 4.29$, $P < 0.05$).

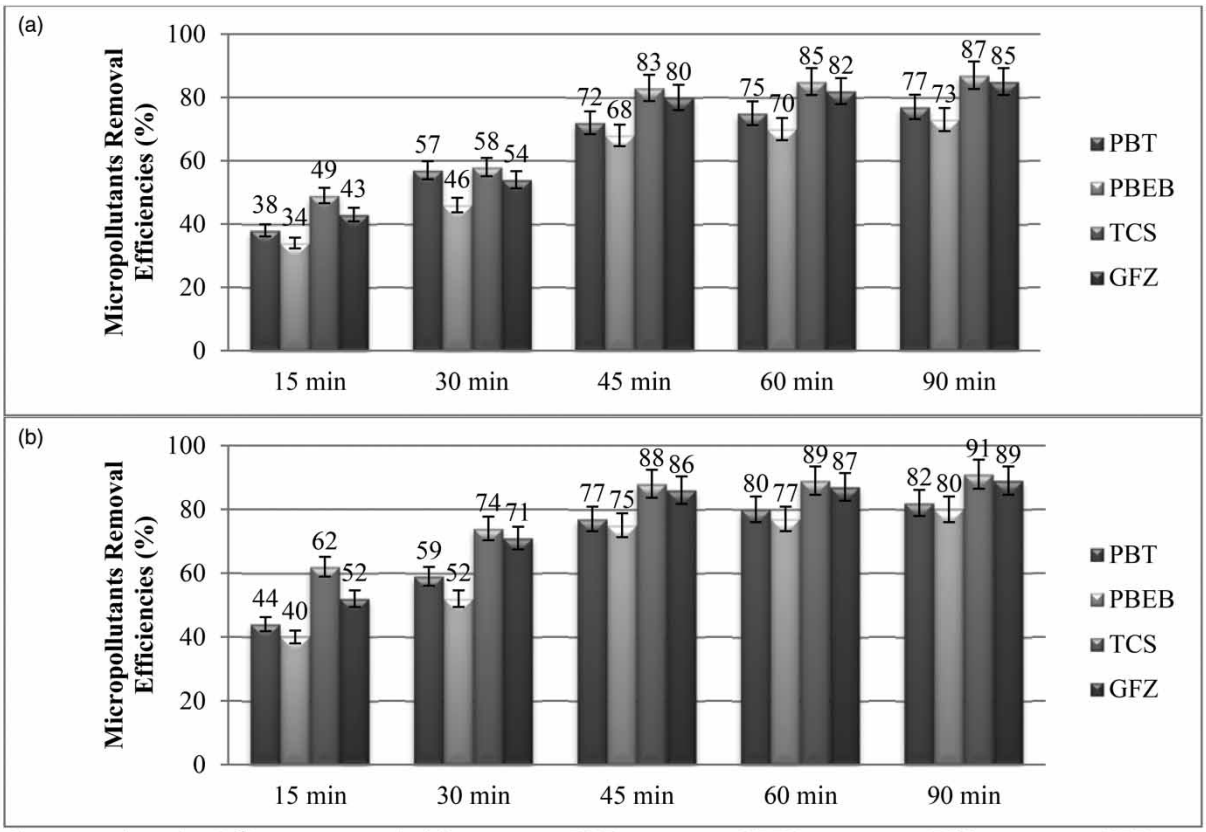
The experiments were also performed using direct photolysis of micropollutants in the absence of nano-TiO_2 and nano-CeO_2 under 210 W UV at 254 nm. As a result, no obvious change in their concentrations within 45 min UV light irradiation was observed (9.0%, 10.0%, 14.2% and 15.9% removals for GFZ, TCS, PBT and PBEB, respectively) (Figure 4(c)). For sole UV exposure, it was found that micropollutants in hospital wastewater with phenol bonds (TCS and GFZ) or brominated bonds (PBT and PBEB) were not easily photolyzed by 254 nm at 210 W UV photons. During photolysis only the photons were generated during UV irradiation instead of generation of hydroxyl radicals ($OH^{\bullet}$). The low removals of GFZ, TCS, PBT and PBEB in photolysis were expected to be achieved mostly by the low number of photons from UV irradiation (Son *et al.* 2009). Similar results were obtained for the direct UV photolysis of TCS and GFZ (Carlson *et al.* 2015). Stamatis *et al.* also found that the removal of 1.0 mg L^{-1} TCS with adsorption and photolysis was low (1.8% and 4.9%, respectively) with 550 mg L^{-1} TiO_2 at an irradiation intensity of 700 W m^{-2} (Stamatis *et al.* 2014). The ANOVA multiple test statistic showed a linear regression between physicochemical properties and removals of micropollutants by photolysis (R = 0.84), although this regression was not significant ($P = 0.15$, $\alpha = 0.05$). The Kruskal–Wallis one way test showed that photolysis had no significant effects on the removal of micropollutants (Kruskal–Wallis ANOVA, $\chi^2 = 16.14$, $P > 0.05$).

Photodegradation of GFZ, TCS, PBT and PBEB

Effect of irradiation time on the photodegradation of GFZ, TCS, PBT and PBEB. According to the previous studies given in the literature and from our preliminary studies it was decided to use a 0.25 g L^{-1} nano-TiO_2 and nano-CeO_2 concentration at a 120 W UV power. The photocatalytic experiments performed with nano-TiO_2 showed that 45 min is the optimum irradiation time for the maximum photocatalytic removal of GFZ (80%), TCS (83%), PBT (72%) and PBEB (68%) at 25 °C at a pH of 7.00 (Figure 5(a)). Any further increase in irradiation time decreased all the micropollutants' photo-removals because of the deactivation of active sites by the deposition of by-products. Neves reported that the increasing of irradiation time from 1 h to 5 h positively affected the 0.01 g L^{-1} TCS removal (from 68% to 78%) at a pH value of 7.00 with 0.50 g L^{-1} TiO_2 with UV (Neves 2014). It is important to note that the TCS photodegradation yields in our study were higher than the data obtained by Neves although they were obtained with half of the nanoparticle dose and four times the irradiation time. Also, the photocatalytic experiments performed with nano-CeO_2 showed that 45 min was the optimum irradiation time for the maximum photocatalytic removals of GFZ (86%), TCS (88%), PBT (77%) and PBEB (75%) with 0.25 g L^{-1} nano-CeO_2 concentration at 120 W power at 25 °C and at a pH of 7.00 (Figure 5(b)). It is widely accepted that UV excitation leads to the generation of electron (e^-_{CB}) – hole (h^+_{VB}) pairs on the nano-TiO_2 and nano-CeO_2 surface. These charges will react with water molecules and result in $OH^{\bullet}$. The hydroxyl radicals oxidize the micropollutant molecules and cause the latter to decompose and mineralize to water and to carbon dioxide. ANOVA test statistics showed that a linear regression between irradiation time and micropollutant photo-removals was observed by increasing the irradiation time from 15 min to 60 min (R = 0.89) and this correlation was significant ($P = 0.50$). The Kruskal–Wallis one way test showed that the increased length of time up to 60 min had a significant effect on micropollutant removals (Kruskal–Wallis ANOVA, $\chi^2 = 1.12$, $p < 0.05$). A significant regression between photodegradation yields of micropollutants and irradiation time for higher than 45 min (60 and 90 min) (R = 0.23) was not observed and this correlation was not significant (P = 12.07, $\alpha = 0.05$) (Kruskal–Wallis ANOVA, $\chi^2 = 16.78$, $p < 0.05$).

The lower photodegradation yields in PBEB and PBT compared to GFZ and TCS can be attributed to the difficulties in separating the five brominated groups with methyl and ethyl during consecutive reductive debromination as reported by Lee & Kwon (2016). Their high log K_{ow} and low solubilities and their hydrophobicities compared to GFZ and TCS resulted in low removals. It was reported that debromination is a main photochemical reaction pathway for NBFRs (Covaci *et al.* 2011). During photooxidation, intramolecular elimination of HBr from PBEB and PBT can subsequently generate lower brominated compounds via consecutive debromination (Covaci *et al.* 2011). Higher photodegradation yields of TCS were observed (87%) to produce several intermediates including a dioxin congener (2,8-dichlorodibenzodioxin) under UV with TiO_2 via dechlorination as reported by Bianco *et al.* (2015). The separation of chlorinated and phenolic groups photodegraded the TCS to CO_2 and water. Wang *et al.* (2017) found that TCS was photodegraded with a yield of 78% under 130 W UV power while the photodegradation was enhanced to 89% with 1–5 kGy gamma irradiation,

Downloaded from http://iwaponline.com/wst/article-pdf/76/10/2603/242040/wst076102603.pdf
by guest

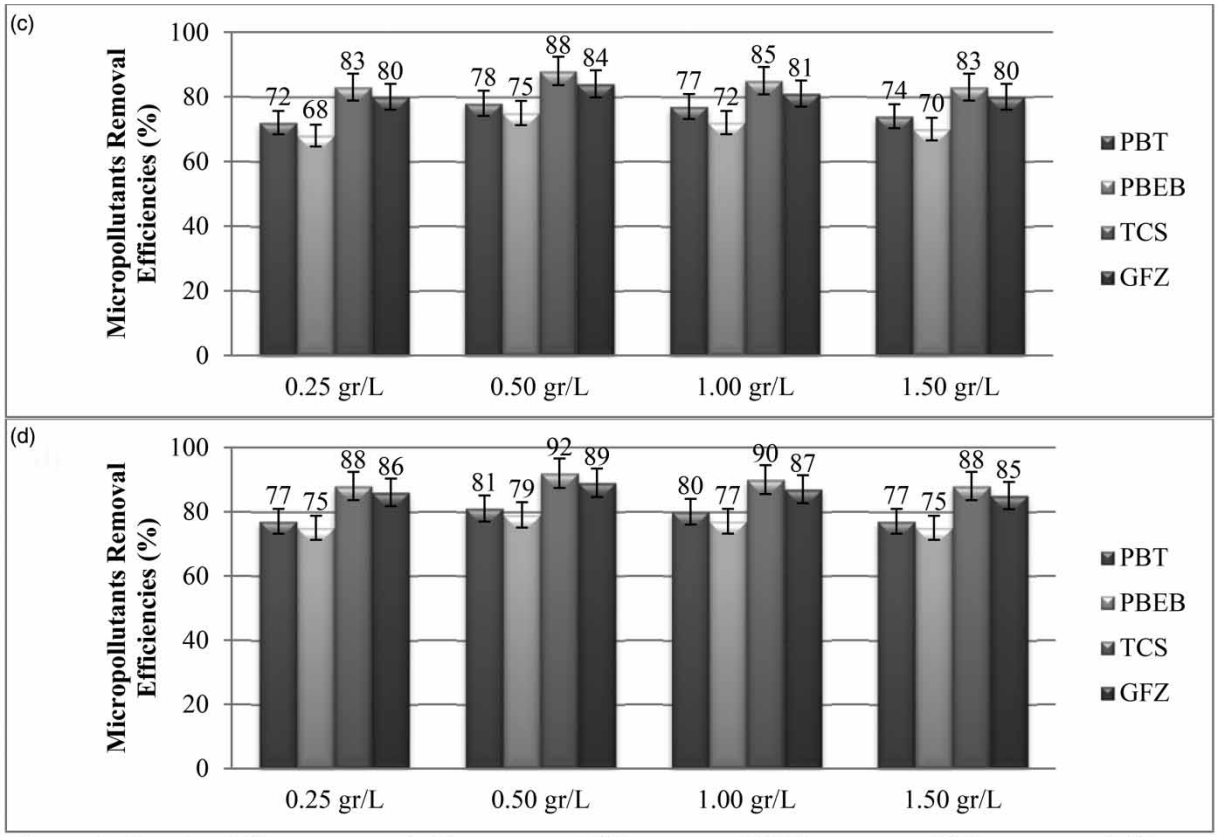


Concentrations (μg L^{-1})	t (min)	PBT	PBEB	TCS	GFZ
Influent	15 30 45 60 90	2.31	3.28	860.00	53.30
Effluent for nano-TiO_2	15	1.43	2.18	438.60	30.20
	30	1.00	1.78	361.20	24.52
	45	0.65	1.05	146.20	10.66
	60	0.58	0.98	129.00	9.59
	90	0.53	0.88	111.80	8.00
Effluent for nano-CeO_2	15	1.30	1.98	326.80	25.40
	30	0.95	1.58	220.00	15.52
	45	0.53	0.82	103.20	7.46
	60	0.46	0.75	94.00	6.90
	90	0.41	0.66	77.40	5.70

Figure 5 | (a) Effect of time on the photodegradation of GFZ, TCS, PBT and PBEB at 0.25 g L^{-1} nano-TiO_2 , at 120 W, 25 °C and at pH = 7.00. (b) Effect of time on the photodegradation of GFZ, TCS, PBT and PBEB at 0.25 g L^{-1} CeO_2, at 120 W, 25 °C and at pH = 7.00. (c) Effect of nano-TiO_2 on the photodegradation of GFZ, TCS, PBT and PBEB at 45 min, at 120 W, 25 °C and at pH = 7.00, (d) Effect of nano-CeO_2 on the photodegradation of GFZ, TCS, PBT and PBEB at 45 min, at 120 W, at 25 °C and at pH = 7.00. (e) Effect of UV light power on the photodegradation of GFZ, TCS, PBT and PBEB at 45 min at 0.50 g L^{-1} nano-TiO_2 at 25 °C and at pH = 7.00 (f) Effect of UV light power on the photodegradation of GFZ, TCS, PBT and PBEB at 45 min, at 0.50 g L^{-1} nano-CeO_2 at 25 °C and at pH = 7.00. (g) Effect of pH on the photodegradation of GFZ, TCS, PBT and PBEB at 45 min, at 0.50 g L^{-1} nano-TiO_2 at 210 W and at 25 °C. (h) Effect of pH on the photodegradation of GFZ, TCS, PBT and PBEB at 45 min at 0.50 g L^{-1} nano-CeO_2 at 210 W and at 25 °C.

resulting in the mineralization of TCS. When the OH addition attacked the GFZ, transient states of the OH adduct radicals were formed, resulting in the formation of hydroxylated by-products (e.g., GFZ-Pa), followed by further radical oxidation to form stable by-products (GFZ-Pb and -Pd). When the OH addition reaction took place on the ipso aromatic C atom of GFZ-Pa, this ipso-substitution led to stabilized carbon-centered radicals. In

Downloaded from http://iwaponline.com/wst/article-pdf/76/10/2603/242040/wst076102603.pdf
by guest



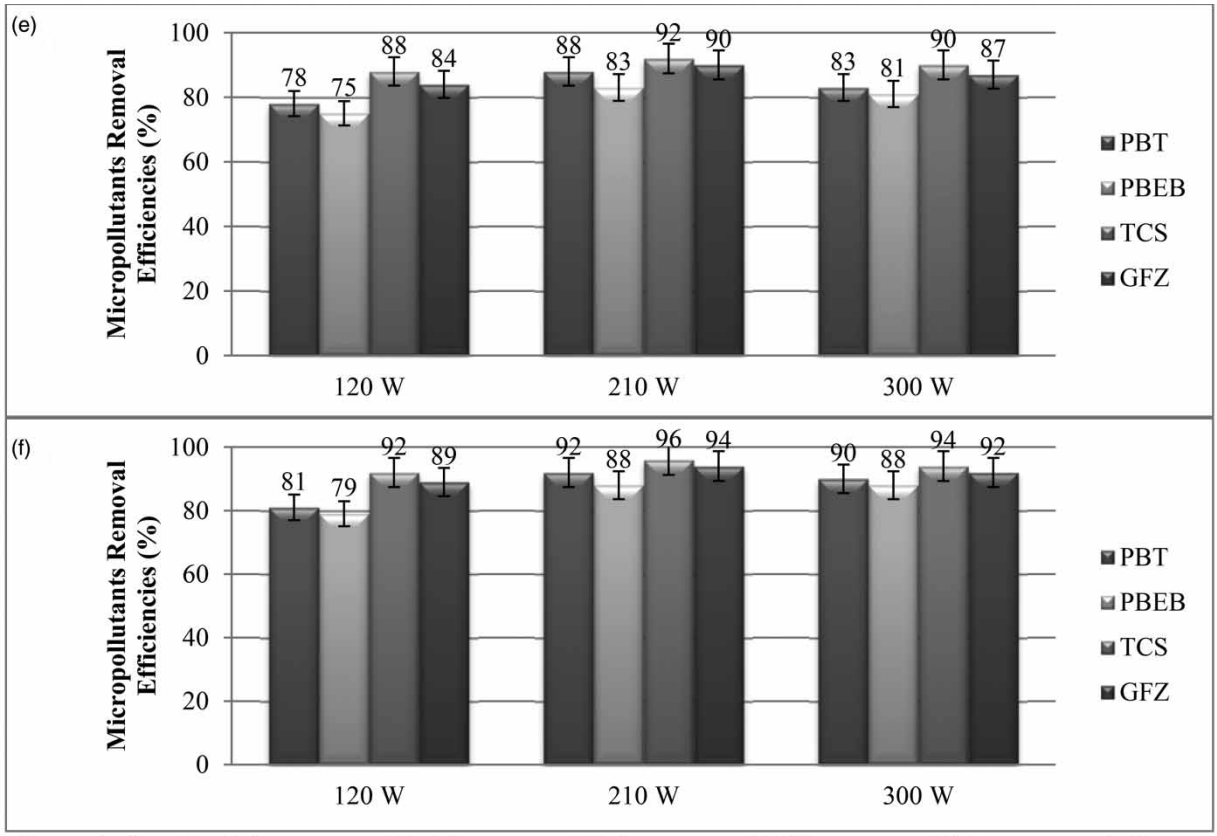
Concentrations (μg L^{-1})	t (min)	PBT	PBEB	TCS	GFZ
Influent	0.25 0.50 1.00 1.50	2.31	3.28	860.00	53.30
Effluent for nano-TiO_2	0.25	0.65	1.05	146.20	10.66
	0.50	0.51	0.82	103.20	8.53
	1.00	0.53	0.92	129.00	10.13
	1.50	0.60	0.98	146.20	10.66
Effluent for nano-CeO_2	0.25	0.53	0.82	103.20	7.46
	0.50	0.44	0.69	68.80	5.86
	1.00	0.46	0.75	86.00	6.93
	1.50	0.53	0.82	103.20	8.00

Figure 5 | Continued.

addition, O-dealkylation reactions caused either side chain cleavage of the parent compound, giving rise to the generation of GFZ-Pc/k (Chen *et al.* 2017). The photo-removals of PBT, PBEB, TCS and GFZ found in this study were higher than in the literature cited above.

Effects of nano-TiO_2 and nano-CeO_2 concentrations on the photodegradation of GFZ, TCS, PBT and PBEB. Photocatalytic removals of 84%, 88%, 78% and 75% were obtained for GFZ, TCS, PBT and PBEB with 0.50 g L^{-1} nano-TiO_2 (Figure 5(c)). Increasing the amount of photocatalysts from 0.25 to 0.50 g L^{-1} resulted in an increase in the photodegradation efficiencies of GFZ, TCS, PBT and PBEB. Among the 0.25, 0.50, 1.00 and 1.50 g L^{-1} nanoparticle concentrations, 0.50 g L^{-1} was determined as the optimum nanoparticle concentration at 120 W power at 25 °C and at a pH of 7.00 for maximum photodegradation yields of micropollutants. The photodegradation yields found for GFZ and TCS were higher than for PBT and PBEB due to their physicochemical properties. Concentrations of nano-TiO_2 and

Downloaded from http://iwaponline.com/wst/article-pdf/76/10/2603/242040/wst076102603.pdf
by guest

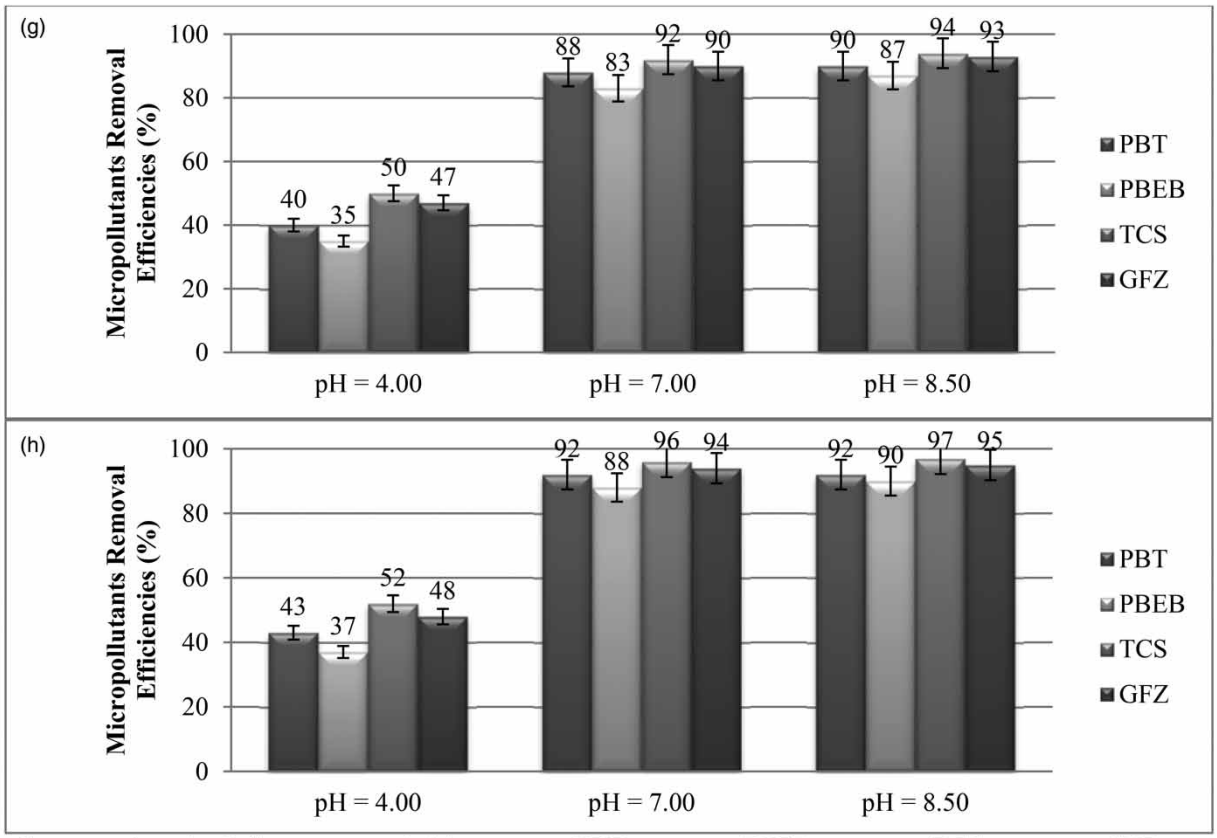


Concentrations (μg L^{-1})	t (min)	PBT	PBEB	TCS	GFZ
Influent	120 210 300	2.31	3.28	860.00	53.30
Effluent for nano-TiO_2	120	0.51	0.82	103.20	8.53
	210	0.28	0.55	68.80	5.33
	300	0.39	0.62	86.00	6.93
Effluent for nano-CeO_2	120	0.44	0.69	68.80	5.86
	210	0.18	0.39	34.40	3.20
	300	0.23	0.39	51.60	4.26

Figure 5 | Continued.

nano-CeO_2 higher than 0.50 g L^{-1} slightly decreased the photodegradation yields of GFZ, TCS, PBT and PBEB. The increase in TiO_2 loading from 0.25 g L^{-1} to 0.50 g L^{-1} provided more binding sites for substrate molecules to adsorb to the TiO_2 surface. At low TiO_2 loading low photodegradation yields were obtained for all the micropollutants since the number of active sites on the surface of the nanoparticle was low and partially exposed to the pollutants. With excessive nano-TiO_2 and nano-CeO_2 loadings (1.00 and 1.50 g L^{-1}), it has been suggested that the TiO_2 particles in the centre of an irradiating vessel may be shielded from the incident UV by other nano-TiO_2 and nano-CeO_2 particles, and thus particles in the center do not contribute significantly to the production of electron (e^-_{CB}) – hole (h^+_{VB}) pairs (Bethi *et al.* 2016). At high TiO_2 concentrations the contacting sites on the surface of the nanocomposite were not fully activated to bind to the micropollutants. Therefore, the photodegradation yields decreased. The optimum concentrations of nano-TiO_2 and nano-CeO_2 were useful both from the economic and the photodegradation efficiency standpoint, because an increase in opacity and light scattering of TiO_2 particles occurred at high concentrations, leading to the decreased passage of UV irradiation through the suspension (Bethi *et al.* 2016). By

Downloaded from http://iwaponline.com/wst/article-pdf/76/10/2603/242040/wst076102603.pdf
by guest



Concentrations (μg L^{-1})	t (min)	PBT	PBEB	TCS	GFZ
Influent	4.00 7.00 8.50	2.31	3.28	860.00	53.30
Effluent for nano-TiO_2	4.00	1.39	2.13	430.00	28.25
	7.00	0.28	0.56	68.80	5.33
	8.50	0.23	0.43	51.60	3.73
Effluent for nano-CeO_2	4.00	1.32	2.07	412.80	27.72
	7.00	0.18	0.39	34.40	3.20
	8.50	0.18	0.33	25.80	2.67

Figure 5 | Continued.

increasing the catalyst concentration to an optimum level, the surface area was increased, leading to an increase in the production of reactive species. However, increased nanoparticle concentrations would also induce greater aggregation of the catalyst and decrease the total active surface area, thereby leading to a reduction in the photocatalytic treatment efficiency. The Kruskal–Wallis one way test showed that significant effects of nanoparticle concentration on the removal of micropollutants were observed as the nanoparticle concentration was raised from 0.25 to 0.50 g L^{-1} (Kruskal–Wallis ANOVA, $\chi^2 = 1.07$, $p < 0.05$). Any further increase of nano-TiO_2 and nano-CeO_2 concentrations (from 0.5 to 1.5 g L^{-1}) did not have a significant effect on micropollutant removals (Kruskal–Wallis ANOVA, $\chi^2 = 17.31$, $p > 0.05$).

Corena studied the effect of TiO_2 concentrations on the photocatalytic removal of GFZ at a pH of 5.00 for an initial GFZ concentration of 2 mg L^{-1} at 100 W UV light power. The increase in TiO_2 concentration from 0.10 g L^{-1} to 1.50 g L^{-1} affected GFZ removal positively because greater surface area and more active sites became available for TiO_2. However, an increase in TiO_2 concentration from 1.50 g L^{-1} to 2.50 g L^{-1} decreased the ability of the UV radiation to reach the TiO_2 surface because a portion of the UV

Downloaded from http://iwaponline.com/wst/article-pdf/76/10/2603/242040/wst076102603.pdf
by guest

light was reduced and scattered by the TiO_2 nanoparticles (Corena 2015). A concentration of 0.50 g L^{-1} nano-CeO_2 gave better results for the photocatalytic removal of GFZ (89%), TCS (92%), PBT (81%) and PBEB (79%) than nano-TiO_2 with 0.50 g L^{-1} at 120 W power at 25 °C and at a pH of 7.00 (Figure 5(d)). This can be attributed to the higher specific surface area of nano-CeO_2 (302 m^2 g^{-1}) with smaller particle sizes compared to TiO_2 (205 m^2 g^{-1}). Balavi *et al.* showed that the photocatalytic activity characteristic of CeO_2 results in it being a proper alternative instead of TiO_2 and ZnO in photocatalytic removal of some colored wastewaters (Balavi *et al.* 2013).

During photodegradation of GFZ, TCS, PBT and PBEB, semiconductor nano-TiO_2 and nano-CeO_2 were excited by photons (hv) and produced pairs of electrons (e^-_{CB}) and holes (h^+_{VB}) in the conduction and valance bands, respectively. The photogenerated electrons (e^-_{CB}) and holes (h^+_{VB}) were able to react with O_2 and OH^- to generate $OH^\bullet$. $OH^\bullet$ tended to attack the carbon atoms with the highest electron density (Yu *et al.* 2006). The steps given below removed the micropollutants from the raw hospital wastewater (Equations (3)–(24)).

(a) Generation of the electron (e^-_{CB}) – hole (h^+_{VB}) pairs:

$$TiO_2/CeO_2 + hv \rightarrow e^-_{CB} + h^+_{VB} \quad (3)$$

(b) Keeping the holes at the valance band:

$$h^+_{VB} + H_2O \rightarrow H^+ + OH^\bullet \quad (4)$$

$$h^+_{VB} + OH^- \rightarrow OH^\bullet \quad (5)$$

(c) Electron (e^-_{CB}) transfer to the conduction band:

$$e^-_{CB} + O_2 \rightarrow {}^\bullet O_2^- \quad (6)$$

$$2\,{}^\bullet O_2^- + 2H^+ \rightarrow H_2O_2 + O_2 \quad (7)$$

$${}^\bullet O_2^- + 2H^+ \rightarrow 2OH^\bullet \quad (8)$$

$$e^-_{CB} + H_2O_2 \rightarrow OH^- + OH^\bullet \quad (9)$$

(d) Oxidation of TCS: The phenol-type intermediates (benzoic acid and phenol) of TCS occurred during photocatalysis due to the formation of $OH^\bullet$ (Son *et al.* 2009). Photodegradation of TCS to CO_2 and H_2O occurred via $OH^\bullet$ according to the following equations (Equations (10)–(13)):

$$C_{12}H_7Cl_3O_2\,(TCS) + OH^\bullet \rightarrow C_6H_4Cl_2O + C_6H_5OH \quad (10)$$

$$C_{12}H_7Cl_3O_2 + OH^\bullet \rightarrow C_6H_4ClOH + C_6H_5OH \quad (11)$$

$$C_{12}H_7Cl_3O_2 + OH^\bullet \rightarrow C_7H_6O_2 + C_6H_5OH \quad (12)$$

$$C_6H_5OH + OH^\bullet \rightarrow CO_2 + H_2O \quad (13)$$

(e) Oxidation of GFZ: Photodegradation of GFZ to CO_2 and H_2O occurred via $OH^\bullet$ and ${}^\bullet O_2^-$ according to the following equations (Equations (14)–(18)) (Chen *et al.* 2017):

$$C_{15}H_{22}O_3\,(GFZ) + OH^\bullet \rightarrow C_{15}H_{23}O_4 \quad (14)$$

$$C_{15}H_{23}O_4 + OH^\bullet \rightarrow C_{15}H_{24}O_5 \quad (15)$$

$$C_{15}H_{24}O_5 + OH^\bullet \rightarrow CO_2 + H_2O \quad (16)$$

$$C_{15}H_{22}O_3 + {}^\bullet O_2^- \rightarrow C_9H_9O_3 \quad (17)$$

$$C_9H_9O_3 + OH^\bullet \rightarrow CO_2 + H_2O \quad (18)$$

(f) Mineralization of PBT and PBEB to CO_2 and H_2O via $OH^\bullet$ and ${}^\bullet O_2^-$ occurred via exciting the bromines according to the following equations, respectively (Equations (19)–(22)) (Chen *et al.* 2012):

$$C_7H_3Br_5\,(PBT) + OH^\bullet \rightarrow 5Br^\bullet + C_7H_2O + H_2 \quad (19)$$

$$C_7H_2O + 7\,{}^\bullet O_2^- \rightarrow 7CO_2 + H_2O \quad (20)$$

$$C_8H_5Br_5\,(PBEB) + OH^\bullet \rightarrow 5Br^\bullet + C_8H_4O + H_2 \quad (21)$$

$$C_8H_4O + 17/2\,{}^\bullet O_2^- \rightarrow 8CO_2 + 2H_2O \quad (22)$$

(g) Conjunction of the charge conductors (electron (e^-_{CB}) – hole (h^+_{VB}) pairs get together and the reaction ends):

$$e^-_{CB} + h^+_{VB} \rightarrow \text{heat} \quad (23)$$

$$e^-_{CB} + OH^\bullet \rightarrow TiO_2/CeO_2 + OH^- \quad (24)$$

Effect of UV light power on the photodegradation of GFZ, TCS, PBT and PBEB. The photocatalytic reactor was

Downloaded from http://iwaponline.com/wst/article-pdf/76/10/2603/242040/wst076102603.pdf
by guest

operated with a 0.50 g L^{-1} nanoparticle (nano-TiO_2 and nano-CeO_2) concentration for 45 min UV irradiation at 25 °C and at a pH of 7.00 at increasing UV light powers (120, 210 and 300 W) in order to determine the optimum UV light power for the maximum micropollutant photodegradation. The micropollutant photodegradations were obtained as 84%, 88%, 78% and 75%, respectively, for 120 W UV light power after 45 min irradiation time at 0.50 g L^{-1} nano-TiO_2 (Figure 5(e)). When the UV light power was increased to 210 W, the micropollutant photodegradation removals reached 90%, 92%, 88% and 83%, respectively, at the same irradiation time (Figure 5(e)). As the UV light power was increased to 300 W the photodegradation yields for GFZ, TCS, PBT and PBEB decreased slightly (Figure 5(e)). In this case, more hydroxyl radicals were available to attack the aromatic rings and the rate of removal increased. For the photocatalytic experiments carried out with nano-CeO_2, the micropollutant photodegradation yields were obtained as 89%, 92%, 81% and 79%, respectively, at 120 W UV light power (Figure 5(f)). The micropollutant photodegradation yields increased significantly when the UV light power was increased to 210 W (Figure 5(f)). Finally when the UV light power was increased to 300 W the photodegradation yields for GFZ, TCS, PBT and PBEB decreased slightly (Figure 5(f)). The optimum UV light power for maximum micropollutant photoremovals was found to be 210 W at 0.50 g L^{-1} nano-TiO_2 and nano-CeO_2 concentrations after 45 min irradiation time at 25 °C at pH = 7.00. Kruskal–Wallis test statistics showed that the UV power significantly increased micropollutant removals, up to 210 W UV power (ANOVA, $\chi^2 = 2.31$, $p < 0.05$). UV power higher than 210 W decreased micropollutant removal ((ANOVA, $\chi^2 = 14.88$, $p > 0.05$).

It should be pointed out that the photodegradation rates of micropollutants mentioned above increased when the UV light irradiation power was increased from 120 W up to 210 W. After 210 W UV power had been reached for a certain period of time, the margin of increase dropped. At this UV power, formation of long-lived intermediate by-products did not accumulate in the solution before their reaction with hydroxyl radical and photo-transformation into carbon dioxide and water (Bai & Acharya 2016). This is the reason for the high photodegradation yields of micropollutants found in this study. The removal yields of the micropollutants mentioned above during the photocatalysis process increased linearly when the UV light power was increased from 120 W to 210 W. The multiple regression analysis showed that a significant linear correlation between GFZ, TCS, PBT, and PBEB photodegradation yields and UV power up to 300 W (R = 0.86) and this regression was significant (P = 0.53, $\alpha = 0.05$). As the UV power was increased to 300 W, the electron (e^-_{CB}) – hole (h^+_{VB}) recombination causes lower effects on the photo-removal yields since some metabolites accumulated and this decreased effective OH radical production, as reported by Caudillo-Flores *et al.* (2016). Ma *et al.* (2016) and Chen *et al.* (2017) found similar results for GFZ photodegradation under 230 W and 298 W powers. Chen *et al.* (2016a, 2016b) mentioned that for a maximum photodegradation kinetic constant an optimum UV power (267 W) was necessary. Covaci *et al.* (2011) and Ezechiás *et al.* (2014) mentioned that optimum UV powers (180–190 W) were necessary for the cleavage of brominated rings in PBEB and PBT from NBFRs since these organics have low volatility, low water solubility, and high log K_{ow} levels.

Effect of pH on the photodegradation of GFZ, TCS, PBT and PBEB. In photocatalysis, pH can affect the reaction of OH radical production from H_2O/OH^- and nano-TiO_2. The photodegradation rates of GFZ, TCS, PBT and PBEB were researched under acidic (pH = 4.00), neutral (pH = 7.00) and alkaline pH (pH = 8.50) conditions after 45 min irradiation time at 210 W UV light power with a nanoparticle concentration of 0.50 g L^{-1} nano-TiO_2 at 25 °C. Under acidic pH (4.00) GFZ, TCS, PBT and PBEB photodegradation yields were 47%, 50%, 40% and 35%, respectively (Figure 5(g)). The photocatalytic yields at neutral pH (7.00) increased (Figure 5(g)). Under alkaline conditions (8.50), GFZ, TCS, PBT and PBEB photodegradation yields reached the maximum (93%, 94%, 90% and 87%, respectively) under the same experimental conditions with the nano-TiO_2 (Figure 5(g)).

The surface of the photocatalyst may become positively or negatively charged depending on the ambient pH. TiO_2 has a point of zero charge at around pH = 6 (Son *et al.* 2009). The surface of the photocatalyst will be positively charged in solutions below this pH and negatively charged above. Therefore, the pH will impact the adsorption of micropollutants on the TiO_2 surface depending on their chemical structure. In this study, it was found that the most efficient pH was 8.50 for this nanoparticle whereas more extreme pH conditions negatively affected the photodegradation yields. This is due to the chemical structure of GFZ and TCS at pH = 8.50. Both the phenoxy and chloro groups on chloro-phenol moieties in GFZ (dissociation constant $pK_a = 8.6$) and dimethyl and phenoxy moieties ($pK_a = 6.1$) in TCS are deprotonated with the overall charge being negative (Son *et al.* 2009). Therefore, because of negative surface charge of TiO_2, maximal photodegradation

Downloaded from http://iwaponline.com/wst/article-pdf/76/10/2603/242040/wst076102603.pdf
by guest

occurs. Similarly, at low pH, both these functional groups are protonated, and hence the overall positive charge of GFZ and TCS results in low photodegradation yields as reported by Martínez-Zapata *et al.* (2013). Molinari *et al.* studied the effect of pH on the photocatalytic degradation of GFZ with UV/TiO_2. They observed that the maximum GFZ photodegradation yield was at alkaline pH values since the TiO_2 surface was charged negatively and the carboxylic group of GFZ was in the anionic form causing a repulsion phenomenon with the TiO_2 nanoparticle (Molinari *et al.* 2008). The Kruskal–Wallis test showed that the effect of pH on micropollutant photodegradation yields was significant (ANOVA, $\chi^2 = 2.03$, $p < 0.05$).

The GFZ, TCS, PBT and PBEB photodegradation yields were lower (48%, 52%, 43% and 37%, respectively) in acidic pH (4.00) compared to neutral pH (7.00) conditions at 0.50 g L^{-1} CeO_2 concentrations for the same operational conditions given for TiO_2 (Figure 5(h)). The photocatalytic yields of GFZ, TCS, PBT and PBEB increased to 95%, 97%, 92% and 90%, respectively, at a pH of 8.50 (Figure 5(h)). The reason for the increase of the photodegradation yields of the four micropollutants at pH = 8.50 can be explained by the hydroxyl radicals being more readily produced at higher pH values. As a result, the larger amount of hydroxyl radicals produced increased the photocatalytic degradation removals, as reported by Chow *et al.* (2012). Son *et al.* reported that the decreasing of photocatalytic removals under acidic conditions is due to inhibition of hydroxyl radical generation (Son *et al.* 2009). Since the pH of the raw hospital wastewater was 8.50, no pH adjustment was needed to achieve maximum GFZ, TCS, PBT and PBEB photodegradation yields with nano-TiO_2 and nano-CeO_2. This would decrease the cost of chemicals used to adjust the pH of hospital wastewater.

Recovery and reuse of nano-TiO_2 and nano-CeO_2

In order to decrease the catalyst cost, recoveries of nano-TiO_2 and nano-CeO_2 were researched in this study. Six sequential treatment steps were investigated in order to determine possible reusability of the TiO_2 and CeO_2 nanoparticles. The TiO_2 and CeO_2 nanoparticles were reused at the optimum experimental conditions (45 min irradiation time, 0.50 g L^{-1} nanoparticle concentration, 210 W UV light power, pH = 8.50 at 25 °C). TCS, GFZ, PBT and PBEB removal efficiencies were taken into consideration to detect the reusability of nano-TiO_2 and nano-CeO_2 throughout the sequential six treatments. After the first treatment step with nano-TiO_2, the maximum removal efficiencies of TCS, GFZ, PBT and PBEB were determined as 94%, 93%, 90% and 87%, respectively (Table 4). After the second treatment step, the removal efficiencies of TCS, GFZ, PBT and PBEB were determined as 92%, 91%, 90% and 86%, respectively (Table 4). The removal efficiencies of TCS, GFZ, PBT and PBEB were obtained as 88%, 88%, 85% and 81%, respectively, after the fifth treatment step. In the sixth treatment step, the removal efficiencies decreased to 80%, 78%, 75% and 74% for TCS, GFZ, PBT and PBEB, respectively (Table 4).

The maximum removal efficiencies of TCS, GFZ, PBT and PBEB were determined as 97%, 95%, 92% and 90%, respectively, after the first treatment step with nano-CeO_2 (Table 4). After the second treatment step, removal efficiencies of TCS, GFZ, PBT and PBEB were obtained as 96%, 93%, 91% and 90%, respectively (Table 4). After the fifth treatment step, the removal efficiencies of TCS, GFZ, PBT and PBEB were determined as 92%, 89%, 86% and 85%, respectively. The removal efficiencies decreased to 86%, 83%, 80% and 79% for TCS, GFZ, PBT and PBEB, respectively after the sixth treatment step (Table 4). The results showed that the nano-TiO_2 and nano-CeO_2 can be used effectively for five sequential runs (the lowest removal efficiency was 81% with nano-TiO_2 and it was 85% with nano-CeO_2 for PBEB at the end of the fifth treatment step) for the photocatalytic treatment of TCS, GFZ, PBT and PBEB from raw hospital wastewater to decrease the cost of treatment.

Table 4 | The utilization of the nano-TiO_2 and nano-CeO_2 for six times for TCS, GFZ, PBT and PBEB removals under optimum experimental conditions (45 min, 0.50 g L^{-1} nano-CeO_2, 210 W UV light power)

	TCS	GFZ	PBT	PBEB
	Removal efficiencies (%) with nano-TiO_2			
1st treatment step	94	93	90	87
2nd treatment step	92	91	90	86
3rd treatment step	92	91	88	84
4th treatment step	90	90	83	83
5th treatment step	88	88	81	81
6th treatment step	80	78	75	74
	Removal efficiencies (%) with nano-CeO_2			
1st treatment step	97	95	92	90
2nd treatment step	96	93	91	90
3rd treatment step	94	93	90	88
4th treatment step	94	91	87	86
5th treatment step	92	89	86	85
6th treatment step	86	83	80	79

Downloaded from http://iwaponline.com/wst/article-pdf/76/10/2603/242040/wst076102603.pdf
by guest

Cost analysis

A cost analysis was carried out for the photocatalytic treatment of TCS, GFZ, PBT and PBEB from 1 m^3 raw hospital wastewater at optimum experimental conditions (45 min irradiation time, 500 g L^{-1} nanoparticle concentration, 210 W UV light power, pH = 8.50 at 25 °C) with nano-TiO_2 and nano-CeO_2. The UV power required was provided using 20 UV lamps. Also, electricity consumption and nanoparticle synthesis costs were considered. The total cost of the photocatalytic treatment of TCS, GFZ, PBT and PBEB from 1 m^3 raw hospital wastewater was found as 8.70 € and 2.28 € at the optimum experimental conditions with nano-TiO_2 and nano-CeO_2, respectively (Table 5). For both nanoparticles, 4×10^{-3} € was spent on 20 UV lamps and 9.5×10^{-2} € was determined as the investment cost. The chemical cost of synthesizing the TiO_2 nanoparticle and electricity consumption cost were only 8.60 €, while the chemical cost to synthesize the CeO_2 nanoparticle and electricity consumption cost were only 2.18 €. The cost analysis for the photodegradation of TCS, GFZ, PBT and PBEB from raw hospital wastewater showed that the photocatalytic removal with nano-CeO_2 is cheaper compared to nano-TiO_2. In this study, the main part of the cost consisted of the chemicals (8.57 € for nano-TiO_2 synthesis and 2.15 € for nano-CeO_2 synthesis). Conducting the studies in sunlight significantly decreased the cost of the study. Since these studies were performed during January and February in the laboratory, the power of the sun was low. Furthermore, a UV light simulator was not used. Preliminary studies showed that photocatalytic experiments' performed in sunlight decreased the total cost by 76%.

No recent literature was found concerning the photocatalytic cost of the micropollutants studied. However, some costs were compared with our data. Zhang *et al.* (2011) calculated that 99 € was needed to treat 500 m^3 of wastewater containing 34 mg L^{-1} methyl orange dye using only 1.9 g L^{-1} TiO_2. Fenoll *et al.* (2012) and Wandre *et al.* (2016) found that the cost of photodegrading 1 m^3 of wastewater containing 12 mg L^{-1} TCS and 20 mg L^{-1} methyl orange was 102 €

Table 5 | Cost analysis for the photocatalytic treatment of TCS, GFZ, PBT and PBEB for 1 m^3 raw hospital wastewater with nano-TiO_2 and nano-CeO_2 at the optimum experimental conditions (45 min, 500 g L^{-1} nanoparticle concentration, 210 W UV light power, pH = 8.50 at 25 °C)

Cost analysis	Photocatalytic treatment of TCS, GFZ, PBT and PBEB with nano-TiO_2	Photocatalytic treatment of TCS, GFZ, PBT and PBEB with nano-CeO_2
UV	1 UV lamp: 0.2×10^{-3} € 20 UV lamp: $20 \times (0.2 \times 10^{-3}$ €$) = 4 \times 10^{-3}$ €	1 UV lamp: 0.2×10^{-3} € 20 UV lamp: $20 \times (0.2 \times 10^{-3}$ €$) = 4 \times 10^{-3}$ €
Photocatalytic reactor Isolated cabin Magnetic stirrer	0.11×10^{-3} €/h → $(0.11 \times 10^{-3}$ €/h$) \times (0.75$ h$) = 8.25 \times 10^{-5}$ € 0.017 €/h → (0.017 €/h) × (0.75 h) = 1.28×10^{-2} € 0.11 €/h → (0.11 €/h) × (0.75 h) = 8.25×10^{-2} €	0.11×10^{-3} €/h → $(0.11 \times 10^{-3}$ €/h$) \times (0.75$ h$) = 8.25 \times 10^{-5}$ € 0.017 €/h → (0.017 €/h) × (0.75 h) = 1.28×10^{-2} € 0.11 €/h → (0.11 €/h) × (0.75 h) = 8.25×10^{-2} €
Electricity consumption	1 UV lamp: 30 W power 1 kWh = 1,000 W 45 min = 0.75 h 1 kWh electricity: 0.06 € (30 W/lamp) × (20 lamps) × (1 kWh/1,000 W) × (0.75 h) × (0.06 €/1 kWh) = 0.03 €	1 UV lamp: 30 W power 1 kWh = 1,000 W 45 min = 0.75 h 1 kWh electricity: 0.06 € (30 W/lamp) × (20 lamps) × (1 kWh/1,000 W) × (0.75 h) × (0.06 €/1 kWh) = 0.03 €
Chemicals	Titanium (IV) chloride ($TiCl_4$) solution (500 mL): 45.92 € Pluronics P123 (1 kg): 150.00 €	Polyoxyethylene octylphenol ether (500 mL): 250.00 € 1-hexanol (500 mL): 75.00 € Cyclohexane (500 mL): 75.00 € Cerium (III) nitrate hexahydrate ($Ce(NO_3)_3.6H_2O$) (125 g): 337.50 €
Nanoparticle synthesis	For 500 g nano-TiO_2: 92 mL $TiCl_4$ solution: 8.45 € 0.80 g P123: 0.12 €	For 500 g nano-CeO_2: 1 mL polyoxyethylene octylphenol ether: 0.50 € 1 mL 1-hexanol: 0.15 € 1 mL cyclohexane: 0.15 € 0.50 g $Ce(NO_3)_3.6H_2O$: 1.35 €
Total cost	4×10^{-3} € + 8.25×10^{-5} € + 1.28×10^{-2} € + 8.25×10^{-2} € + 0.03 € + 8.45 € + 0.12 € = 8.70 €	4×10^{-3} € + 8.25×10^{-5} € + 1.28×10^{-2} € + 8.25×10^{-2} € + 0.03 € + 0.50 € + 0.15 € + 0.15 € + 1.35 € = 2.28 €

Note: Recent euro exchange rate was used to convert Turkish liras to euro (1 TL = 0.302 €).

Downloaded from http://iwaponline.com/wst/article-pdf/76/10/2603/242040/wst076102603.pdf
by guest

and 127 €, respectively, in the presence of 2 g L^{-1} nano-TiO_2 and CeO_2. These costs are higher than our cost of treating the raw wastewater containing the four micropollutants.

CONCLUSIONS

In this study the nano-TiO_2 and nano-CeO_2 were produced under laboratory conditions to photodegrade TCS, GFZ, PBT and PBEB from raw hospital wastewater for the first time in Turkey. XRD analysis showed that the TiO_2 nanoparticle completely originated from the pure anatase phase with a tetragonal crystal structure. The XRD patterns of CeO_2 showed that they had a cubic fluorite structure and exhibited strong agglomeration. The FT-IR spectrum of the TiO_2 nanoparticle showed the bending vibration of OH molecules, the carbonyl peak and stretching vibrations of Ti-OH. The FT-IR spectrum peaks of CeO_2 nanoparticles originated from the (Ce-O) metal–oxygen bond vibrations.

Under optimized operational conditions (45 min irradiation time, 0.50 g L^{-1} nanoparticle concentration, 210 W UV light power, pH = 8.50 at 25 °C) the nano-CeO_2 had a higher photocatalytic activity (97% TCS, 95% GFZ, 92% PBT and 90% PBEB) than nano-TiO_2 (94% TCS, 95% GFZ, 90% PBT and 87% PBEB) to remove these micropollutants from raw hospital wastewater since its pore volume, average size and pore diameter were low with high band gap energy. The slightly lower alkaline pH (8.50) maximized the photo-removals of micropollutants from the raw hospital wastewater. TiO_2-photocatalytic efficiency decreased in acidic conditions by inhibiting the generation of OH radicals. The nano-CeO_2 and nano-TiO_2 used in this study were recovered effectively to be used again with photodegradation yields as high as 85–94% and 83–90%, respectively. The cost of treating the TCS, GFZ, PBT and PBEB from 1 m^3 raw hospital wastewater was 2.28 € with CeO_2 nanoparticles. The results of this study showed that TCS, GFZ, PBT and PBEB in raw hospital wastewaters can be effectively removed with photodegradation by the utilization of nano-CeO_2 and nano-TiO_2 generated under laboratory conditions for the first time in Turkey. This process could be used effectively in other pharmaceutical and hospital wastewater studies, both as pilot projects and as real treatment in the field.

ACKNOWLEDGEMENTS

The authors would like to thank TUBITAK for the PhD dissertation grant given to Gokce Guney on the Priority Section Subjects (Grant number 2211-C Prior Sections; Water; Prior, Specific and Micro Pollutants).

REFERENCES

APHA/AWWA/WEF 2012 *Standard Methods for the Examination of Water and Wastewater*, 22nd edn. American Public Health Association/American Water Works Association/Water Environment Federation, Washington, DC, USA.

Bai, X. & Acharya, K. 2016 Removal of trimethoprim, sulfamethoxazole, and triclosan by the green alga *Nannochloris* sp. *Journal of Hazardous Materials* **315**, 70–75.

Balavi, H., Samadanian-Isfahani, S., Mehrabani-Zeinabad, M. & Edrissi, M. 2013 Preparation and optimization of CeO_2 nanoparticles and its application in photocatalytic degradation of reactive orange 16 dye. *Powder Technology* **249**, 549–555.

Barón, E., Giménez, J., Verborgh, P., Gauffier, P., De Stephanis, R., Eljarrat, E. & Barceló, D. 2015 Bioaccumulation and biomagnification of classical flame retardants, related halogenated natural compounds and alternative flame retardants in three delphinids from Southern European waters. *Environmental Pollution* **203**, 107–115.

Bethi, B., Sonawane, S. H., Bhanvase, B. A. & Gumfekar, S. P. 2016 Nanomaterials-based advanced oxidation processes for wastewater treatment: a review. *Chemical Engineering and Processing* **109**, 178–189.

Bianco, A., Fabbri, D., Minella, M., Brigante, M., Mailhot, G., Maurino, V., Minero, C. & Vione, D. 2015 New insights into the environmental photochemistry of 5-chloro-2-(2,4-dichlorophenoxy)phenol (triclosan): reconsidering the importance of indirect photoreactions. *Water Research* **72**, 271–280.

Carlson, J. C., Stefan, M. I., Parnis, J. M. & Metcalfe, C. D. 2015 Direct UV photolysis of selected pharmaceuticals, personal care products and endocrine disruptors in aqueous solution. *Water Research* **84**, 350–361.

Caudillo-Flores, U., Muñoz-Batista, M. J., Ung-Medina, F., Alonso-Núñez, G., Kubacka, A., Cortés, J. A. & Fernández-García, M. 2016 Effect of the anatase–rutile contact in gas phase toluene photodegradation quantum efficiency. *Chemical Engineering Journal* **299**, 393–402.

Channei, D., Nakaruk, A. & Phanichphant, S. 2017 Photocatalytic degradation of dye using CeO_2/SCB composite catalysts. *Spectrochimica Acta Part A: Molecular and Biomolecular Spectroscopy* **183**, 218–224.

Chen, Y., Li, J., Liu, L. & Zhao, N. 2012 Polybrominated diphenyl ethers fate in China: a review with an emphasis on environmental contamination levels, human exposure and regulation. *Journal of Environmental Management* **113**, 22–30.

Chen, L., Wang, Z., Wang, Z. & Gu, X. 2016a Influence of humic acid on the photolysis of triclosan in different dissociation forms. *Water Air and Soil Pollution* **227** (9). DOI 10.1007/s11270-016-3024-7.

Chen, L., Wang, Z., Cao, S., Gu, X., Gong, S. & Shen, Z. 2016b Impact of humic acid on the photo-induced toxicity of

Downloaded from http://iwaponline.com/wst/article-pdf/76/10/2603/242040/wst076102603.pdf
by guest

triclosan. *Water Air and Soil Pollution* **227** (7). DOI 10.1007/s11270-016-2940-x.

Chen, P., Wang, F., Chen, Z. F., Zhang, Q., Su, Y., Shen, L., Yao, K., Liu, Y., Cai, Z., Lv, W. & Liu, G. 2017 Study on the photocatalytic mechanism and detoxicity of gemfibrozilby a sunlight-driven TiO_2/carbon dots photocatalyst: the significant roles of reactive oxygen species. *Applied Catalysis B: Environmental* **204**, 250–259.

Chokwe, T. B., Okonkwo, J. O., Sibali, L. L. & Ncube, E. J. 2015 An integrated method for the simultaneous determination of alkylphenol ethoxylates and brominated flame retardants in sewage sludge samples by ultrasonic-assisted extraction, solid phase clean-up, and GC-MS analysis. *Microchemical Journal* **123**, 230–236.

Chow, K. L., Man, Y. B., Zheng, J. S., Liang, Y., Tam, N. F. Y. & Wong, M. H. 2012 Characterizing the optimal operation of photocatalytic degradation of BDE-209 by nano-sized TiO_2. *Journal of Environmental Sciences* **24** (9), 1670–1678.

Chowdhury, S. & Balasubramanian, R. 2014 Recent advances in the use of graphene-family nanoadsorbents for removal of toxic pollutants from wastewater. *Advances in Colloid and Interface Science* **204**, 35–56.

Corena, J. 2015 *Heterogeneous Photocatalysis for the Treatment of Contaminants of Emerging Concern in Water*. PhD thesis, Worcester Polytechnic Institute, Massachusetts, USA.

Covaci, A., Harrad, S., Abdallah, M. A. E., Ali, N., Law, R. J., Herzke, D. & De Wit, C. A. 2011 Novel brominated flame retardants: a review of their analysis, environmental fate and behaviour. *Environment International* **37**, 532–556.

Cristale, J., Quintana, J., Chaler, R., Ventura, F. & Lacorte, S. 2012 Gas chromatography/mass spectrometry comprehensive analysis of organophosphorus, brominated flame retardants, by-products and formulation intermediates in water. *Journal of Chromatography A* **1241**, 1–12.

Cristale, J., Katsoyiannis, A., Sweetman, A. J. & Jones, K. C. 2013 Occurrence and risk assessment of organophosphorus and brominated flame retardants in the River Aire (UK). *Environmental Pollution* **179**, 194–200.

Diwan, V., Tamhankar, A. J., Khandal, R. K., Sen, S., Aggarwal, M., Marothi, Y., Iyer, R. V., Sundblad-Tonderski, K. & Stalsby-Lundborg, C. 2010 Antibiotics and antibiotic-resistant bacteria in waters associated with a hospital in Ujjain, India. *BMC Public Health* **10**, 414–422.

Elsherif, Z. A., Abas, S. S., Abdelwahab, M. H. & El-Weshahy, S. 2013 Determination of gemfibrozil and fenofibrate in pharmaceuticals in presence of their degradation products. *International Journal of Pharmacy and Pharmaceutical Sciences* **5** (3), 886–896.

Ezechiáš, M., Covino, S. & Cajthaml, T. 2014 Ecotoxicity and biodegradability of new brominated flame retardants: a review. *Ecotoxicology and Environmental Safety* **110**, 153–167.

Fang, Y., Karnjanapiboonwong, A., Chase, D. A., Wang, J., Morse, A. N. & Anderson, T. A. 2012 Occurrence, fate, and persistence of gemfibrozil in water and soil. *Environmental Toxicology and Chemistry* **31**, 550–555.

Farahmandjou, M., Zarinkamar, M. & Firoozabadi, T. P. 2016 Synthesis of cerium oxide (CeO_2) nanoparticles using simple CO-precipitation method. *Revista Mexicana de Física* **62**, 496–499.

Fenoll, J., Flores, P., Hellín, P., Martínez, C. M. & Navarro, S. 2012 Photodegradation of eight miscellaneous pesticides in drinking water after treatment with semiconductor materials under sunlight at pilot plant scale. *Chemical Engineering Journal* **204–206**, 54–64.

García, A., Delgado, L., Torà, J. A., Casals, E., González, E., Puntes, V., Font, X., Carrera, J. & Sánchez, A. 2012 Effect of cerium dioxide, titanium dioxide, silver, and gold nanoparticles on the activity of microbial communities intended in wastewater treatment. *Journal of Hazardous Materials* **199–200**, 64–72.

Grenni, P., Patrolecco, L., Ademollo, N., Tolomei, A. & Caracciolo, A. B. 2013 Degradation of gemfibrozil and naproxen in a river water ecosystem. *Microchemical Journal* **107**, 158–164.

Hassani, A., Khataee, A., Karaca, S., Karaca, C. & Gholami, P. 2017 Sonocatalytic degradation of ciprofloxacin using synthesized TiO_2 nanoparticles on montmorillonite. *Ultrasonics Sonochemistry* **35**, 251–262.

Hu, A., Zhang, X., Luong, D., Oakes, K. D., Servos, M. R., Liang, R., Kurdi, S., Peng, P. & Zhou, Y. 2012 Adsorption and photocatalytic degradation kinetics of pharmaceuticals by TiO_2 nanowires during water treatment. *Waste and Biomass Valorization*. DOI 10.1007/s12649-012-9142-6.

Hu, X., Zhu, Q., Gu, Z., Zhang, N., Liu, N., Stanislaus, M. S., Li, D. & Yang, Y. 2017 Wastewater treatment by sonophotocatalysis using PEG modified TiO_2 film in a circular photocatalytic-ultrasonic system. *Ultrasonics Sonochemistry* **36**, 301–308.

Krkošek, W. H., Koziar, S. A., White, R. L. & Gagnon, G. A. 2011 Identification of reaction products from reactions of free chlorine with the lipid-regulator gemfibrozil. *Water Research* **45**, 1414–1422.

Lee, H. J. & Kwon, J. H. 2016 Evaluation of long-range transport potential of selected brominated flame retardants with measured 1-octanol–air partition coefficients. *Bulletin of the Korean Chemical Society* **37** (10), 1696–1702.

Ma, J., Lv, W., Ping, C., Lu, Y., Wang, F., Li, F., Yao, K. & Liu, G. 2016 Photodegradation of gemfibrozil in aqueous solution under UV irradiation: kinetics, mechanism, toxicity, and degradation pathways. *Environmental Science and Pollution Research* **23**, 14294–14306.

Maaroof, M. & Uysal, Y. 2014 Use the extended activated sludge process to remove triclosan (TCS) from wastewater treatment plant. *KSU Journal of Engineering Sciences* **17**, 20–26.

Martínez-Zapata, M., Aristizábal, C. & Penuela, G. 2013 Photodegradation of the endocrine-disrupting chemicals 4n-nonylphenol and triclosan by simulated solar UV irradiation in aqueous solutions with Fe(III) and in the absence/presence of humic acids. *Journal of Photochemistry and Photobiology A: Chemistry* **251**, 41–49.

Molinari, R., Caruso, A., Argurio, P. & Poerio, T. 2008 Degradation of the drugs gemfibrozil and tamoxifen in pressurized and de-pressurized membrane photoreactors using suspended polycrystalline TiO_2 as catalyst. *Journal of Membrane Science* **319**, 54–63.

Montaseri, H. & Forbes, P. B. C. 2016 A review of monitoring methods for triclosan and its occurrence in aquatic environments. *Trends in Analytical Chemistry* **85**, 221–231.

Downloaded from http://iwaponline.com/wst/article-pdf/76/10/2603/242040/wst076102603.pdf
by guest

Neves, A. 2014 *Photochemical Degradation of Triclosan: A Comparison between Different Light Sources*. PhD thesis, Faculdade De Ciencias E Tecnologia Universidade Nova De Lisboa, Lisbon, Portugal.

Petrie, B., McAdam, E. J., Lester, J. N. & Cartmell, E. 2014 Obtaining process mass balances of pharmaceuticals and triclosan to determine their fate during wastewater treatment. *Science of the Total Environment* **497–498**, 553–560.

Phuruangrat, A., Thongtem, T. & Thongtem, S. 2017 Effect of NaOH on morphologies and photocatalytic activities of CeO_2 synthesized by microwave-assisted hydrothermal method. *Materials Letters* **193**, 161–164.

Quinn, G. P. & Keough, M. J. 2002 *Experimental Design and Data Analysis for Biologists*. Cambridge University Press, New York.

Ravishankar, T. N., Ramakrishnappa, T., Nagaraju, G. & Rajanaika, H. 2015 Synthesis and characterization of CeO_2 nanoparticles via solution combustion method for photocatalytic and antibacterial activity studies. *Chemistry Open*. DOI: 10.1002/open.201402046.

Son, H. S., Ko, G. & Zoh, K. D. 2009 Kinetics and mechanism of photolysis and TiO_2 photocatalysis of triclosan. *Journal of Hazardous Materials* **166**, 954–960.

Stamatis, N., Antonopoulou, M., Hela, D. & Ioannis Konstantinou, I. 2014 Photocatalytic degradation kinetics and mechanisms of antibacterial triclosan in aqueous TiO_2 suspensions under simulated solar irradiation. *Journal of Chemical Technology and Biotechnology* **89**, 1145–1154.

Sun, R. X., Luo, X. J., Tan, X. X., Tang, B., Li, Z. R. & Mai, B. X. 2015 An eight year (2005–2013) temporal trend of halogenated organic pollutants in fish from the Pearl River Estuary, South China. *Marine Pollution Bulletin* **93**, 61–67.

Tambat, S., Umale, S. & Sontakke, S. 2016 Photocatalytic degradation of Milling Yellow dye using sol–gel synthesized CeO_2. *Materials Research Bulletin* **76**, 466–472.

Tang, Y., Yang, M., Gao, H., Li, J. & Wang, G. 2016 A facile approach for fabrication of TiO_2 hierarchical nanostructures and their photocatalytic properties. *Colloids and Surfaces A: Physicochemical and Engineering Aspects* **508**, 184–191.

Tohidi, F. & Cai, Z. 2017 Fate and mass balance of triclosan and its degradation products: comparison of three different types of wastewater treatments and aerobic/anaerobic sludge digestion. *Journal of Hazardous Materials* **323**, 329–340.

Wandre, T. M., Gaikwad, P. N., Tapase, A. S., Garadkar, K. M., Vanalakar, S. A., Lokhande, P. D., Sasikala, R. & Hankare, P. P. 2016 Sol–gel synthesized TiO_2–CeO_2 nanocomposite: an efficient photocatalyst for degradation of methyl orange under sunlight. *Journal of Materials Science: Materials in Electronics* **27** (1), 825–833.

Wang, H., Li, Y., Zhang, Y., Chen, J., Chu, G. & Shao, L. 2015 Preparation of CeO_2 nano-support in a novel rotor–stator reactor and its use in Au-based catalyst for CO oxidation. *Powder Technology* **273**, 191–196.

Wang, S., Yin, Y. & Wang, J. 2017 Enhanced biodegradation of triclosan by means of gamma irradiation. *Chemosphere* **167**, 406–414.

Wu, J. P., Guan, Y. T., Zhang, Y., Luo, X. J., Zhi, H., Chen, S. J. & Mai, B. X. 2010 Trophodynamics of hexabromocyclododecanes and several other non-PBDE brominated flame retardants in a freshwater food web. *Environmental Science & Technology* **44**, 5490–5495.

Xie, M., Nghiem, L. D., Price, W. E. & Elimelech, M. 2012 Comparison of the removal of hydrophobic trace organic contaminants by forward osmosis and reverse osmosis. *Water Research* **46**, 2683–2692.

Xu, Y., Wang, C., Hou, J., Wang, P., You, G., Miao, L., Lv, B. & Yang, Y. 2017 Effects of cerium oxide nanoparticles on the species and distribution of phosphorus in enhanced phosphorus removal sequencing batch biofilm reactor. *Bioresource Technology* **227**, 393–397.

Yu, J. C., Kwong, T. Y., Luo, Q. & Cai, Z. 2006 Photocatalytic oxidation of triclosan. *Chemosphere* **65**, 390–399.

Zhang, H., Xu, P., Du, G., Chen, Z., Oh, K., Pan, D. & Jiao, Z. 2011 A facile one-step synthesis of TiO_2/graphene composites for photodegradation of methyl orange. *Nano Research* **4** (3), 274–283.

First received 22 March 2017; accepted in revised form 10 July 2017. Available online 24 July 2017

Downloaded from http://iwaponline.com/wst/article-pdf/76/10/2603/242040/wst076102603.pdf
by guest